Lawrence Smith

Final Report

submitted to

NATIONAL AERONAUTICS AND SPACE ADMINISTRATION
GEORGE C. MARSHALL SPACE FLIGHT CENTER, ALABAMA 35812

September 18, 1992

for Contract NAS 8 - 36955
Delivery Order 128

entitled

Development of Advanced Seal Verification

by
Gary L. Workman Ph.D.
Principal Investigator

Susan E. Kosten
Research Associate
and
Mustafa A. Abushagur, Ph.D.
Associate Professor

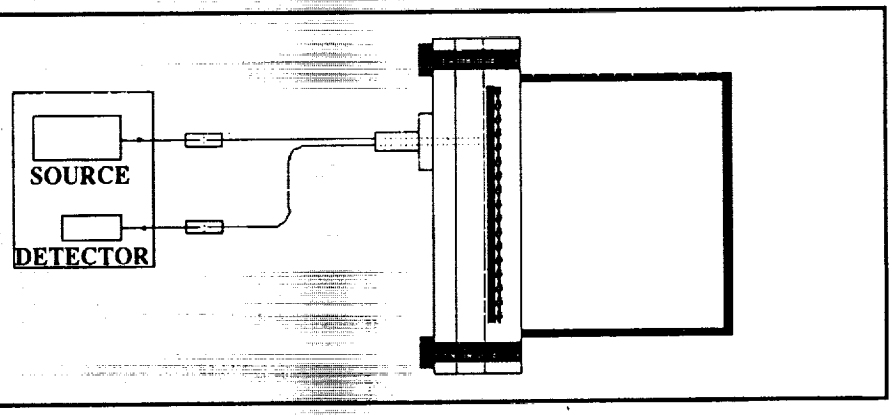

Materials Processing Laboratory
Center for Automation & Robotics
University of Alabama in Huntsville
Huntsville, Alabama 35899

TABLE OF CONTENTS

1.0 Introduction

The development of optical fibers as a communications medium has revolutionized man's ability to transmit and receive information. Combining the capacity for multi-wavelength transmission simultaneously and allowing for high frequency fidelity. the optical fiber is already replacing copper wire and provides an amazing framework for the communications industry to grow for the future. It should be noted that it has taken several decades of research and development to build up man's ability to manufacture reliable communications systems from optical fibers, transmitters, detectors, and the accompanying telecommunication sub-systems. Needless to say, that research has paid off nicely and further research into optical fibers and applications continues at a very high rate.

A new application arena for optical fibers as smart sensors has been evolving over the last few years due to the ability to engineer specific responses from certain types of signal sources into an optical fiber system. This use of optical fibers as sensors has evolved from a large amount of work in characterizing optical fibers for communication applications. In order to develop optical fiber technology for long distance communications, researchers had to perform a substantial amount of work in understanding where losses occur in optical fiber transmission and how to correct for them. It is interesting to note that many of the detrimental characteristics of optical fibers for communications activity turns out to provide our ability to monitor an external parameter, such as pressure or temperature. Consequently many of the early theoretical papers dealing with characterization of optical fibers for communications also defines those characteristics which may be useful for sensors.

The purpose of this research is to develop a technique to monitor and insure seal integrity with a sensor that has no active elements to burn-out during a long duration activity, such as a leakage test or especially during a mission in space. The original concept proposed for this work is that by implementing fiber optic sensors, changes in the integrity of a seal can be monitored in real time and at no time should the optical fiber sensor fail. The electrical components which provide optical excitation and detection through the fiber are not part of the seal; hence, if these electrical components fail, they can be easily changed out with breaking the seal. The optical connections required for the concept to work does present a functional problem to work out. The utility of the optical fiber sensor for seal monitoring should be general enough that the degradation of a seal can be determined before catastrophic failure occurs and appropriate action taken.

In the research reported here, two parallel efforts were performed in determining the feasibility of using optical fiber sensors for seal verification. In one study, Dr. M. Abushagur supervised research on interferometric measurements of the mechanical response of the optical fiber sensor to seal integrity in his optical fiber laboratory in the Electrical and Computer Engineering Department. The second group under Dr. G. Workman's supervision, designed the implementation of the optical fiber to a typical vacuum chamber and performed feasibility studies on microbend experiments in the vacuum chamber. We also attempted to quantify the amount of pressure actually being applied to the optical fiber using Finite Element analysis software by Algor.

2.0 Experimental Approaches

An exploratory project of this nature required that UAH take a number of approaches into the use of optical fibers as sensors because of the diverseness of the phenomena associated with optical fibers. In developing the capability of the research group to implement the optical fiber systems in order to measure responses to pressure variations, many new laboratory skills were learned. In particular, these skills are necessary in order to determine how easily optical fiber sensors can be incorporated into an aerospace system by relatively untrained personnel. This concept is very important in evaluating what impact optical fibers sensors may have in pressure monitoring and seal leakage on space platforms.

Several very good journal articles and books describe how optical fibers work in transmitting light efficiently for optical communications purposes and also how this phenomena can be used to sense certain types of environmental parameters.[1 - 4] It is to be noted that a very large effort by the Naval Research Laboratories was performed in the early 1980's to determine if optical fiber sensors could be used for efficient underwater acoustic sensors.[5] Much of the current knowledge about optical fiber sensors evolved from this program.

In addition to simple pressure measurements made with the optical fiber sensors explored in this work, we felt that there was a need to experiment with an actual vacuum chamber in order to verify the physical requirements for retrofitting and/or implementing an o-ring seal monitor. For this purpose a small vacuum chamber was constructed by Morgan Research to provide verification of the ability of the optical fiber sensor to monitor pressure measurements on a small scale. The small vacuum chamber provided a convenient testbed to develop our

capabilities in handling the optical fibers in o-ring glands and defining what physical characteristics needed to be considered in retrofitting an o-ring gland. This small vacuum chamber also provided a useful test fixture to check the experimental determinations of Dr. Abushagur's sensor techniques, the microbending technique, and the finite element model. It is important to keep in mind that the tests reported here were retrofitted implementations.

A different design concept would be utilized in designing an optical fiber seal monitor from scratch, such as embedding the optical fiber into the seal and modifications to the buffer material of the optical fiber. Embedding the optical fiber in the sealing material would change the dimensions of the milled groove for the optical fiber. The groove for this arrangement would not have to be a graduated groove to a depth of 0.15 inches. It would only need to be approximately 0.012 inches deep depending of the optical fiber outer diameter. A similar concept of embedding a material, a metal wire, in the sealing material has been performed by a company called Bal-Seal. Another type of seal that could be considered for embedding the optical fiber is the gask-o-seal. For this arrangment the no machining would be necessary on the sealing faces. Figures 1 and 2 are the drawings of the small chamber built by Morgan Research, showing how one has to design for the entrance and exit of the optical fiber within the o-ring gland area when the optical fiber is retrofitted.

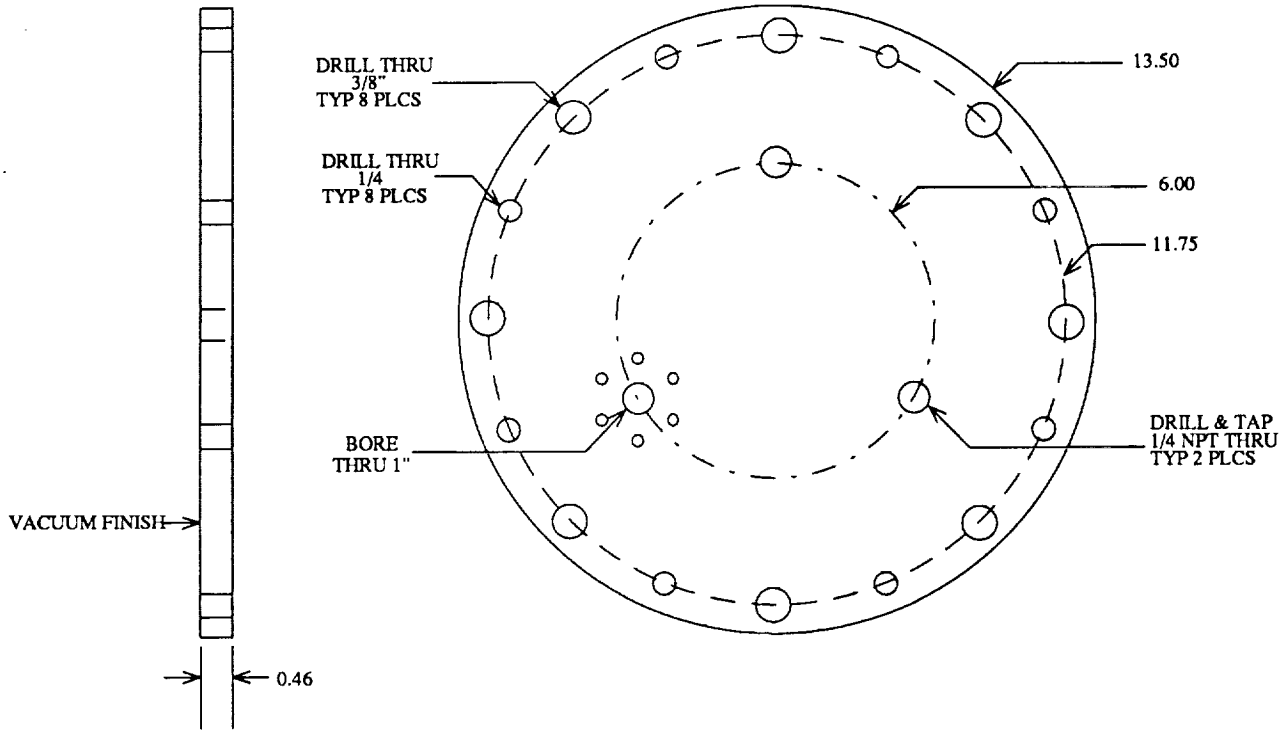

Figure 1. Small vacuum chamber top cover plate.

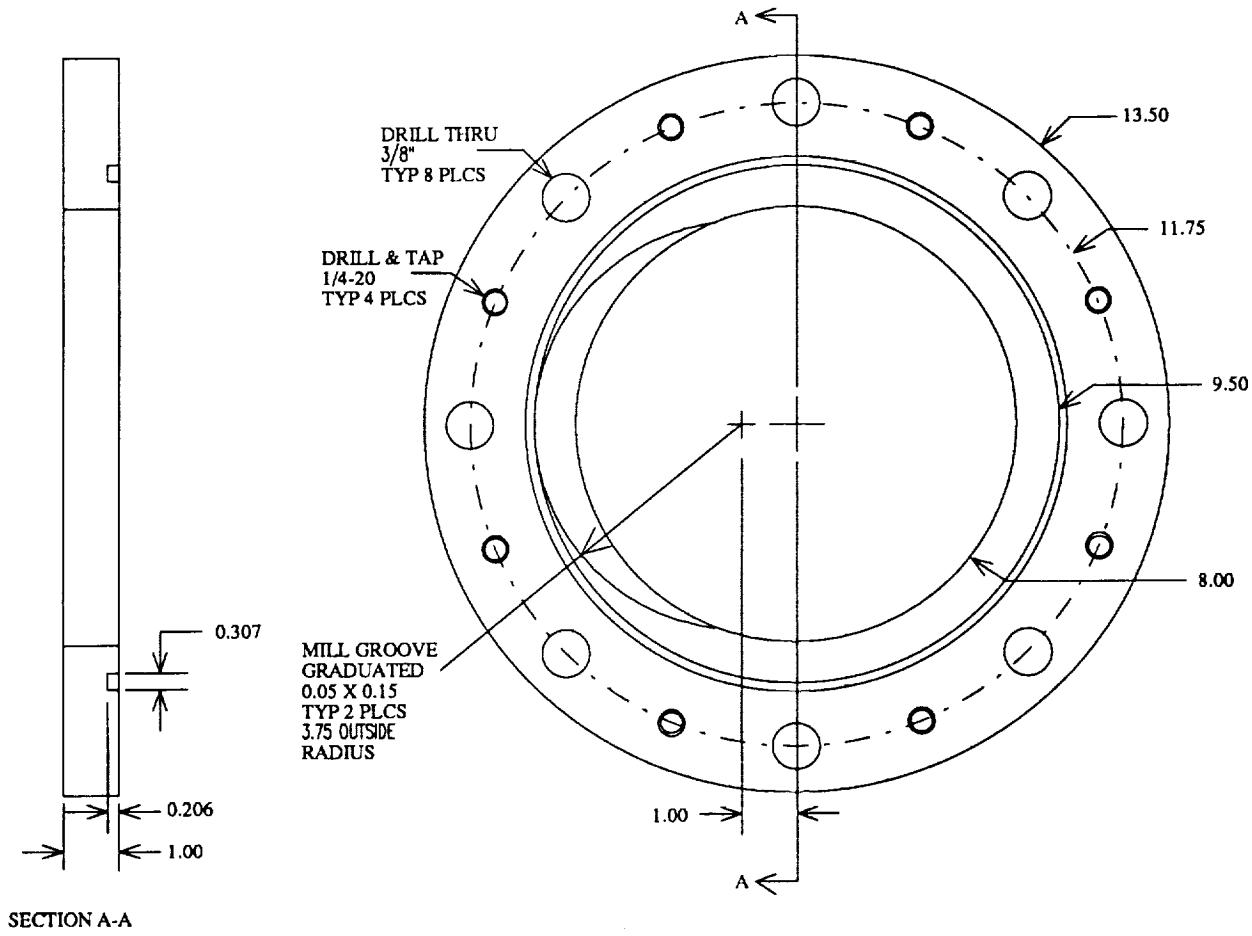

Figure 2. Small vacuum chamber bottom.

2.1 Analytical Modeling

In the earlier stages of this project, it was anticipated to use the Algor finite element analysis program to model the o-ring sensor configuration and determine the actual forces applied to the optical fiber sensor. It was anticipated that the results of the modeling would also enable determination of the best placement of the optical fiber in the groove and possibly the number of fibers to be placed in the groove. Test data coupled with the finite element analysis would then allow one to characterize the pressures observed by the fiber. Several months were used working with the Algor staff including training at the Algor facilities to try to better understand how to model the o-ring sensor configuration. It was determined that the Algor software had

difficulty modeling this system without implementing many stipulations due to the large differences in the modulus of the two materials, i.e. the aluminum fixture and the o-ring. The ultimate goal is still to be able to determine the correct placement of the optical fiber sensor to achieve the desired sensitivity in conjunction with the most accurate results. The models that were generated using Algor's finite element analysis can be found in Section 3.1.

Calculations were made to determine the amount of distortion losses in the fiber due to the microbending of the fiber. It can be shown that as the radius of the core increases while the radius of the outer diameter stays constant, the amount of lost light increases. Which proves the microbending theory of higher order modes being propagated into the buffer material of the fiber. It also shows how the number of spirals or deformations also increases the amount of light lost. Results from the calculations can also be found in Section 3.1.

A numerical model of the lateral pressure actually being applied to the fiber was also calculated for the Corning fiber with different core and buffer radius. In this equation, the lateral pressure is determined by Poisson's ratio, Young's modulus, radius of the core, primary and secondary coatings, and the hydrostatic pressure applied to the fiber. It can be shown that in order to maximize the microbending losses the thickness, Young's modulus, and Poisson's ratio of the secondary coating should be decreased but the Young's modulus and Poisson's ratio of the primary coating should be increased. Calculations for the lateral pressure applied to the core of the fiber for various hydrostatic pressures can be found in Section 3.1.

2.2 Monitoring Techniques

2.2.1 Mach-Zehnder Fiber Interferometer

A very common optical arrangement for determining small changes in materials characteristics is called the Mach-Zehnder interferometer. This optical arrangement allows one to determine very minute changes in the index of refraction of a material using interference fringes formed by a coherent light source traveling along two different paths before being combined in one image plane. Hence knowing the wavelength of the light, the fringes are displaced according to the change in path length effected by the change in the index of refraction of the material under study. This technique has been used frequently in studying crystal growth in microgravity due to the sensitivity of the technique.

The technique is directly applicable to pressure measurement as shown by Hocker[5]. Since optical fibers are frequently composed of silica, which is birefringent; then one experiences an equivalent change due to polarization effects from pressure and temperature changes in an optical fiber configured as an interferometer. Diagrams of the Mach-Zehnder Fiber interferometer are shown in the Appendix, which contains the report from Dr. Abushagur.

2.2.2 Polarization

Most of the early work on acoustic sensors were performed with optical fiber interferometers which depended on the phase change caused by pressure fluctuations experienced by one leg of the interferometer. In this implementation, normally single-mode fibers are employed with normally the ability to propagate symmetrically two mutually perpendicular polarization states. If the two legs of the interferometer are equal in length and uniformly consistent then the polarization effects caused by the birefringence of the silica would be identical, allowing for differences in pressure or temperature caused by external forces to be observed. In practice however, there appear to be distinct differences in optical fibers and the symmetric polarization effects are not always observed. More generally, there is a beat frequency of the two polarization states which causes the observed polarization state to be constantly changing and hence making this measurement difficult. There are solutions which are available; however, it does make implementation of this concept difficult. This phenomena was observed in this work and is discussed in the appendix.

2.2.3 Microbending

One technique that was experimented with in the second phase of the contract is a technique called microbending. Microbending losses in optical transmission occurs when the optical fiber is mechanically deformed perpendicular to its axis. This mechanical deformation causes higher-order optical modes in the core to be transmitted through the core-cladding interface in an amount proportional to the fiber deformation. The high-order optical modes are rays of light that escape the core of the fiber and enter the cladding of the fiber and some even exit the cladding of the fiber. They are created because the angle of incidence is greater then the critical angle therefore it is transmitted out of the core into the cladding. The microbend sensor is most sensitive with a multimode fiber, for both graded index or step index varieties. This enhanced sensitivity is due to the fact that multimode fibers allow several modes of light to travel through the fiber simultaneously rather than the single mode fiber, which only allows one mode to

propagate at a time. The multimode fiber allows more total light to propagate and hence has more light to work with in setting up the detection scheme.

This configuration is much simpler then the interferometric system described earlier. There are less components and temperature is not a concern. Figure 3 shows the complete configuration of the optimal microbend fiber sensor system.

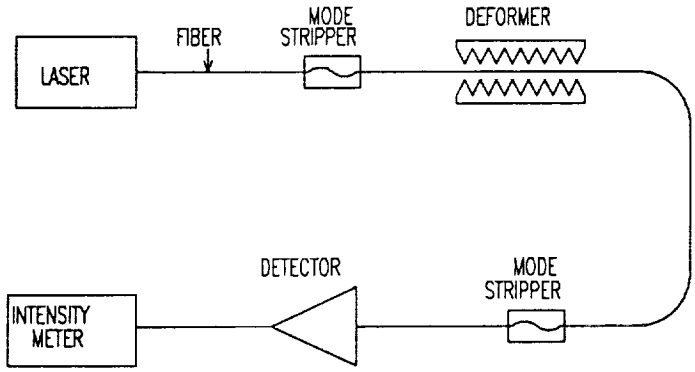

Figure 3. Optical Fiber Microbend System.

The two mode strippers are simply the fiber stripped to the bare core and a index matching liquid placed on the fiber. This removes all of the high order modes that are propagating in the cladding. The mode mixer is simply fusion splicing a piece of multimode step index fiber between two pieces of multimode graded index fiber which attempts to equalize the power in all modes, simulating a fully filled launch which promotes a more repetitive system.

For our system, the microbend sensor consists of one single multimode optical fiber that is twisted in a circular configuration. See Figure 4 below.

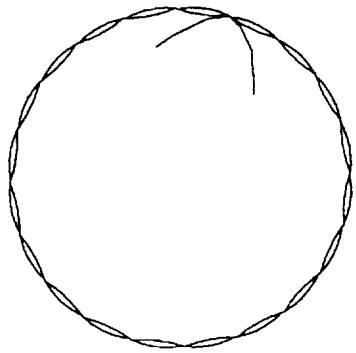

Figure 4. Microbend Circular Spiral Configuration.

The fiber was twisted in a circular configuration because there needed to be some device that acts like the deformer that would not create a leak in the seal. The twist is important in that it provides a very simple arrangement for deformation and requires not external structural elements to be inserted into the o-ring gland. This fiber was then placed along the inside wall of the o-ring groove. A cross sectional picture of the configuration can be seen below.

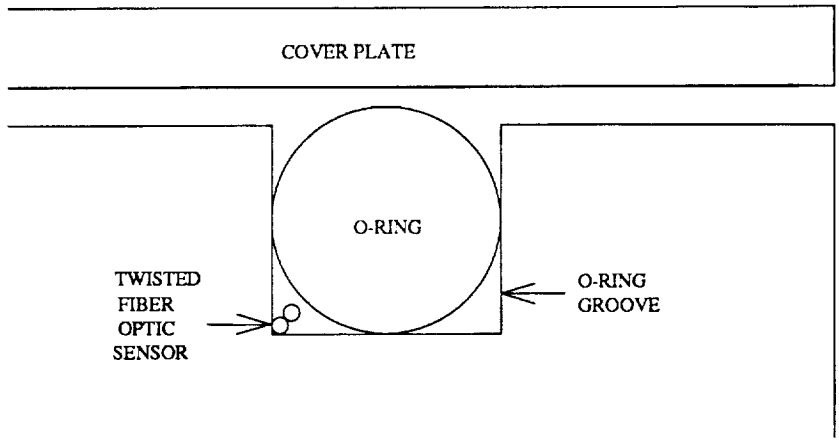

Figure 5. Microbend fiber placement.

The first item to determine before testing began was the type of fiber to be used. Several companies were contacted to attain multimode fiber samples. The samples received can be found below.

Company	Fiber	Core	Cladding	Jacket	NA	Attenuation 850 nm	Attenuation 1300 nm
Corning	62.5/125/250 CPC3	62.5	125	250	0.275	3.0 - 3.2	0.7 - 0.9
Corning	85/125/250 CPC3	85	125	250	0.26	2.8 - 3.5	0.7 - 1.5
Newport	F-MLD	100	140	500	0.3	4.5	2
Newport	F-MMD	62.5	125	500	0.275	3	1
CermOptech	UV100/110P	100	110	130	0.22	~5	?
Fiberguide Ind		300	330	430			
Fiberguide Ind		300	400	500			

The fiber selected for microbending applications must have high attenuation losses in order to allow the light to escape the core when it is deformed, but if the attenuation losses are too great

then even the slightest amount of pressure would allow all of the light to escape. Therefore, the characteristics affecting the sensitivity of the microbend sensor needs to be analyzed.[3] The sensitivity of the sensor is a function of the spatial frequency or the number of deformations for a given length of fiber. Sensitivity is determined by the change in light transmitted in the fiber, ΔT, for a given change in force, ΔF. The greater the ratio $\Delta T/\Delta F$, the greater the sensitivity. If we modify this expression to include a deformation factor, ΔX, the expression would then become

$$\frac{\Delta T}{\Delta F} = \frac{\Delta T}{\Delta X} \times \frac{\Delta X}{\Delta F}$$

The parameter, $\Delta T/\Delta X$ is the sensitivity of the fiber to microbending losses, while $\Delta X/\Delta F$ depends on the spatial frequency and design of the deformer. The ratio $\Delta T/\Delta X$ can be maximized by a small numerical aperture (NA), a large number of deformations, optimum deformer spacing, large ratio of core diameter to fiber diameter, and use of fiber with a graded-index profile. In contrast, $\Delta X/\Delta F$ can be maximized by the use of a small diameter fiber, few deformations, a larger deformer spacing, and a highly compressible fill fluid.

3.0 Experimental Results

3.1 Analytical Results

For the analytical modeling, the system was modeled with the top flange cover and the bottom of the chamber with an 0.25 inch o-ring. Gap elements were placed between the nodes of the contact surfaces to act as interface elements between two faces of a structure in free space. Boundary conditions were added to act as rigid support nodes. A force was placed on top surface of the cover plate to simulate the squeeze and on the right top surface of the o-ring (the bold line) to simulate the forces acting on the o-ring. A thin layer of rubber was added to the aluminum plates at the mating surfaces of the o-ring to add stability to the system due to the large differences in the modulus of the two materials. Figure 6 is the Algor model before analysis. Figure 7 shows the model after analysis with the linear processor. Once the modeling was behaving correctly in the linear portion of the Algor program, it was converted to the non-linear portion of the program. Difficulties were again discovered in the non-linear portion of the program. The gap elements had to be changed to beam elements and decoded as two separate files then combined into one. It appeared after speaking with the Algor staff that this

model was presently beyond their capabilities without implementing many stipulations. Updates to their software are still being received from Algor and continued work has been done on the model in anticipation that newer versions may handle the problem better.

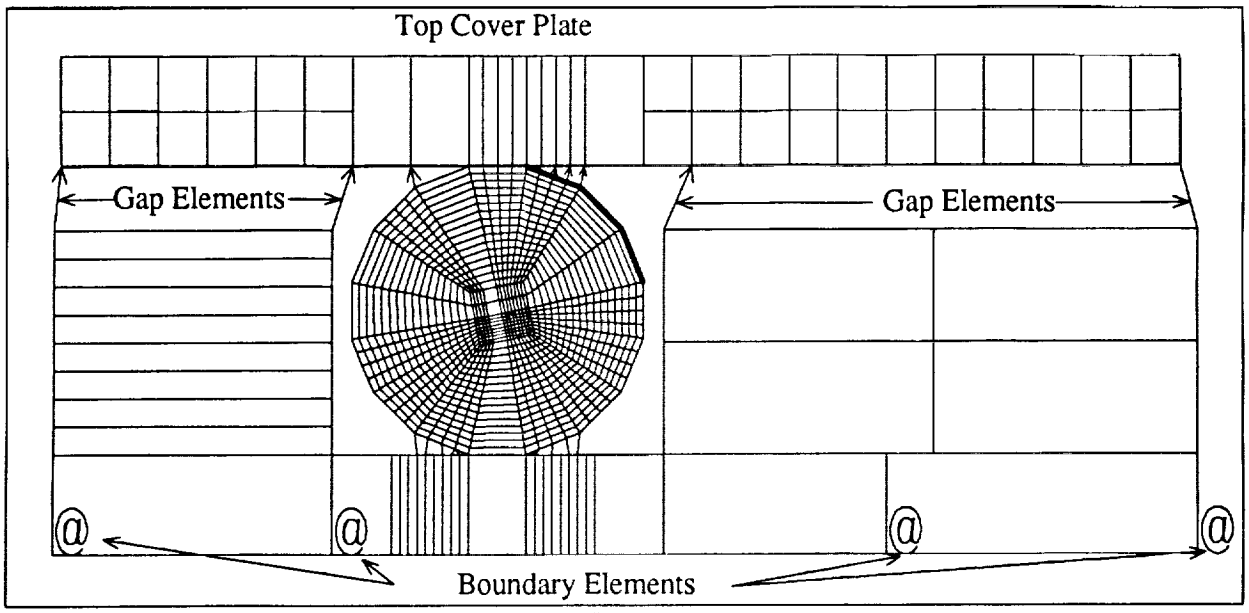

Figure 6. Algor Linear Finite Element Model.

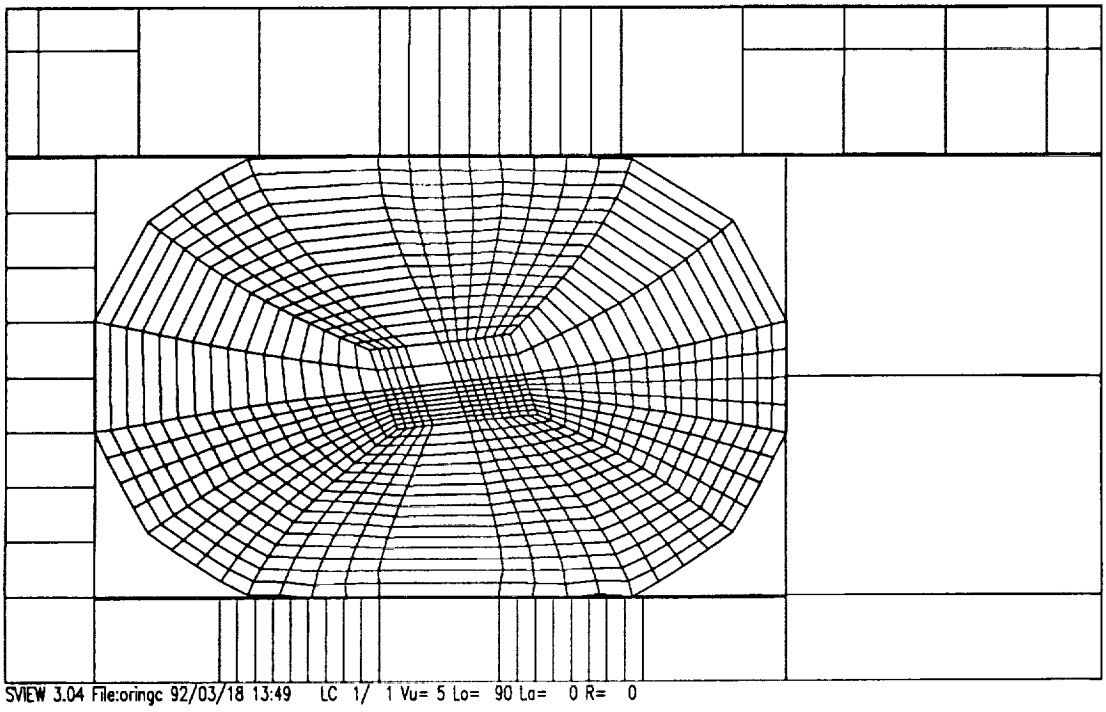

Figure 7. Algor Deformed Linear Finite Element Model.

Calculations using Mathcad were performed to determine the amount of distortion loss in an optical fiber due to microbending the fiber. The results are shown below. This particular calculation was made using a Corning fiber with a fused silica core and a Acrylic coating. Sensitivity of the system is a function of many parameters including the spatial frequency, Young's Modulus and diameter of the core and buffer material, and frequency or wavelength of the light propagating.

Determination of Distortion Losses with Varying Core Diameters

x_a = Distortion loss per spiral in dB

a = Fiber Core Radius in micrometers

b = Fiber Radius in micrometers

D = Relative Index Difference

E_e = Modulus of the Encapsulating Material in kg/mm^2

E_f = Modulus of the Fused Silica in kg/mm^2

h = RMS Bump Height in micrometers

$a := 31..75$

$b := 125$

$\Delta := .01$

$kgEe := 10$

$h := 250$

$Ef := 7200$

$N := 0..20$

$$x_a := 0.9 \cdot h^2 \cdot \left(\frac{1}{b^6}\right) \cdot \left(\frac{1}{\Delta}\right) \cdot \left(\frac{a^2}{\Delta}\right)^2 \cdot \left(\frac{kgEe}{Ef}\right)^{\frac{3}{2}}$$

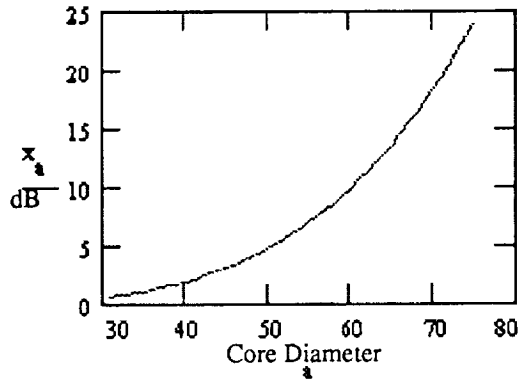

The graph above shows how the radius of the core effects the amount of loss in the fiber. The graph grows exponentially as the radius of the core increases. This equation states that at a core diameter of 100 micrometers the loss in decibels would be 4.77 dB per spiral. Therefore, for an input intensity of 1 watt the output intensity would be

$$10 * \log_{10}(I / I_o) = \text{Loss in dB}$$
$$10 * \log_{10}(1 \text{ watt} / I_o) = 4.77 \text{ dB}$$
$$I_o = 0.33 \text{ Watts}$$

where I is the input intensity and I_O is the output intensity. In contrast for a fiber with a core diameter of 84 microns the loss is 2.375 dB per spiral or deformation. Thus giving an output intensity of 0.58 watts per 250 micron high deformation. Therefore, the light intensity has been almost cut in half after one deformation.

Now, taking the figures of loss per deformation calculation of the loss for 15 spirals or any given number of spirals can be calculated. The graph below in takes the results from the first graph and looks at how the number of deformations increase the loss.

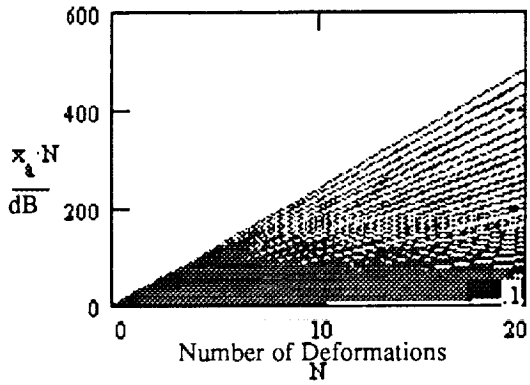

Each line represents a different core radius. As the core reaches its maximum value of 75 micrometers the loss reaches its maximum value at 483 decibels with twenty deformations which transforms to a zero output intensity for an input intensity of 1 watt. This amount of loss is far to great for this application. Therefore, the number of deformations or core radius should be decrease or a fiber with a different buffer material selected.

A numerical model of the lateral pressure actually being applied to the fiber was also calculated for the Corning fiber with different core and buffer radius. In this equation, the lateral pressure is determined by looking at Poisson's ratio, Young's modulus, radius of the core, primary and

secondary coatings, and the hydrostatic pressure applied to the fiber. It can be shown that in order to maximize the microbending losses the thickness, Young's modulus, and Poisson's ratio of the secondary coating should be decreased but the Young's modulus and Poisson's ratio of the primary coating should be increased.

Corning 62.5/125/250

V1 = Poisson's Ratio of the primary coating.
V2 = Poisson's Ratio of the secondary coating.

$\gamma 1 = r_0 / r_1$ = Radius of the core divided by the radius of the primary coating.

$\gamma 2 = r_1 / r_2$ = Radius of the primary coating divided by the radius of the secondary coating.

E1 = Young's modulus of the primary coating.
E2 = Young's modulus of the secondary coating.

P = Hydrostatic pressure (psi).

x_p = Lateral pressure on the fiber.

V1 := .35 E1 := 10000000 P := 0 .. 14.7
V2 := .35 E2 := 1200000000

γ1 := 0.5
γ2 := 0.5

$$x_p := \frac{4\cdot(1 - V1)\cdot(1 - V2)\cdot P}{\frac{E2}{E1}\cdot\frac{(1 + V1)}{(1 + V2)}\cdot(1 - 2\cdot V1)\cdot\left[(1 - \gamma 1^2)\cdot(1 - \gamma 2^2) + \left[\left[1 - (2\cdot V1\cdot\gamma 1^2) + \gamma 1^2\right]\cdot(1 - 2\cdot V2\cdot\gamma 2^2 + \gamma 2^2)\right]\right.}$$

x_p
0
0.027
0.055
0.082
0.109
0.137
0.164
0.191
0.219
0.246
0.273
0.301
0.328
0.355
0.383

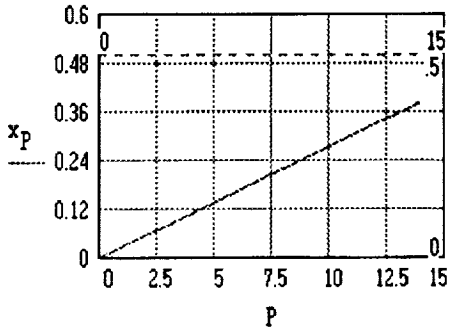

Corning 85/125/250

$\nu 1$ = Poisson's Ratio of the primary coating.
$\nu 2$ = Poisson's Ratio of the secondary coating.

$\gamma 1 = r_0 / r_1$ = Radius of the core divided by the radius of the primary coating.

$\gamma 2 = r_1 / r_2$ = Radius of the primary coating divided by the radius of the secondary coating.

E1 = Young's modulus of the primary coating.
E2 = Young's modulus of the secondary coating.

P = Hydrostatic pressure.

x_p = Lateral pressure on the fiber.

V1 := .35 E1 := 10000000 P := 0 .. 14.7
V2 := .35 E2 := 1200000000

$\gamma 1$:= 0.68
$\gamma 2$:= 0.5

$$x_p := \frac{4\cdot(1-V1)\cdot(1-V2)\cdot P}{\frac{E2}{E1}\cdot\frac{(1+V1)}{(1+V2)}\cdot(1-2\cdot V1)\cdot\left[(1-\gamma 1^2)\cdot(1-\gamma 2^2)+\left[\left[1-\left(2\cdot V1\cdot\gamma 1^2\right)+\gamma 1^2\right]\cdot\left(1-2\cdot V2\cdot\gamma 2^2+\gamma 2^2\right)\right.\right.}$$

x_p
0
0.029
0.058
0.087
0.115
0.144
0.173
0.202
0.231
0.26
0.288
0.317
0.346
0.375
0.404

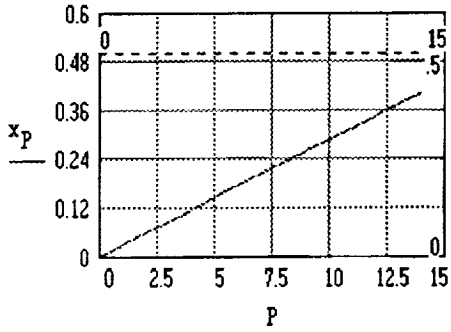

Corning 100/140/250

V1 = Poisson's Ratio of the primary coating.
V2 = Poisson's Ratio of the secondary coating.

$\gamma 1 = r_0 / r_1$ = Radius of the core divided by the radius of the primary coating.

$\gamma 2 = r_1 / r_2$ = Radius of the primary coating divided by the radius of the secondary coating.

E1 = Young's modulus of the primary coating.
E2 = Young's modulus of the secondary coating.

P = Hydrostatic pressure.

x_p = Lateral pressure on the fiber.

V1 := .35 E1 := 10000000 P := 0.. 14.7
V2 := .35 E2 := 1200000000

γ1 := 0.71428571
γ2 := 0.56

$$x_p := \frac{4\cdot(1 - V1)\cdot(1 - V2)\cdot P}{\frac{E2}{E1}\cdot\frac{(1 + V1)}{(1 + V2)}\cdot(1 - 2\cdot V1)\cdot\left[(1 - \gamma 1^2)\cdot(1 - \gamma 2^2) + \left[\left[1 - (2\cdot V1\cdot\gamma 1^2) + \gamma 1^2\right]\cdot(1 - 2\cdot V2\cdot\gamma 2^2 + \gamma 2^2\right.\right.}$$

x_p
0
0.029
0.059
0.088
0.118
0.147
0.176
0.206
0.235
0.264
0.294
0.323
0.353
0.382
0.411

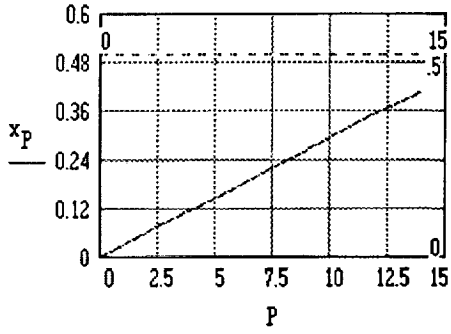

When a comparison is made between the three fibers with the same Poisson's ratio and Young's modulus the lateral pressure on the core is greater for the larger diameter fiber. For example, at 14.7 psi the lateral pressure on the Corning 62.5/125/250 fiber is 0.383 psi but on the Corning

100/140/250 fiber the lateral pressure is 0.411 psi. This represents a 4 percent increase in the lateral pressure seen by the core of the latter.

3.2 Microbend Sensor Results

Initial testing of the microbend concept consisted of setting up different fibers obtained from various vendors in the configuration mentioned in Section 2.2.3 using a Helium-Neon laser, varying number of spirals and circle diameters to change the spatial frequency, known weights, and a photo diode detector. The weights were placed on the spiral microbend fiber and the output intensity was monitored.

In the first test, a comparison was made with four fibers, the Corning 85/125/250 micron fiber, Corning 62.5/125/250 micron fiber, Newport F-MLD and the CeramOptech 100/110/130 micron fiber. All three fibers were placed in a 5.5 inch diameter circular configuration with 10 spirals. Weights were then placed on the fiber ranging from 0 grams to 1000 grams.

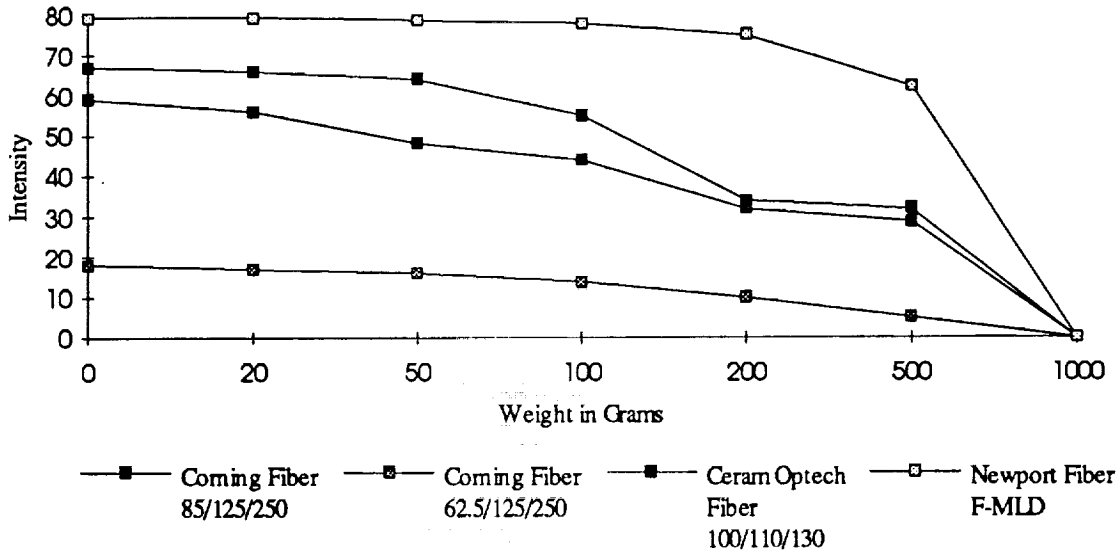

Figure 8. Comparison of the range of light lost due to the force applied.

As it can be seen the sensitivity of the fiber to the weight and the dynamic range varies considerably between the different fibers. This difference in sensitivity can be attributed to many different factors including the numerical aperture, core size, ratio of core size to fiber diameter, and buffer material for instance which were discussed above in the mathematical modeling. It is apparent from the data tested, that the CeramOptech 100/110/130 micron fiber had the largest dynamic range. With the Corning 85/125/250 CPC3 having a more linear output investigation of the spatial frequency of this fiber were performed. This test consisted of changing the spatial frequency of the spirals by changing the diameter of the circle. Using fifteen spirals the diameter was changed from six inches to five inches to three and three quarter inches. The results from this test can be found in Figure 9.

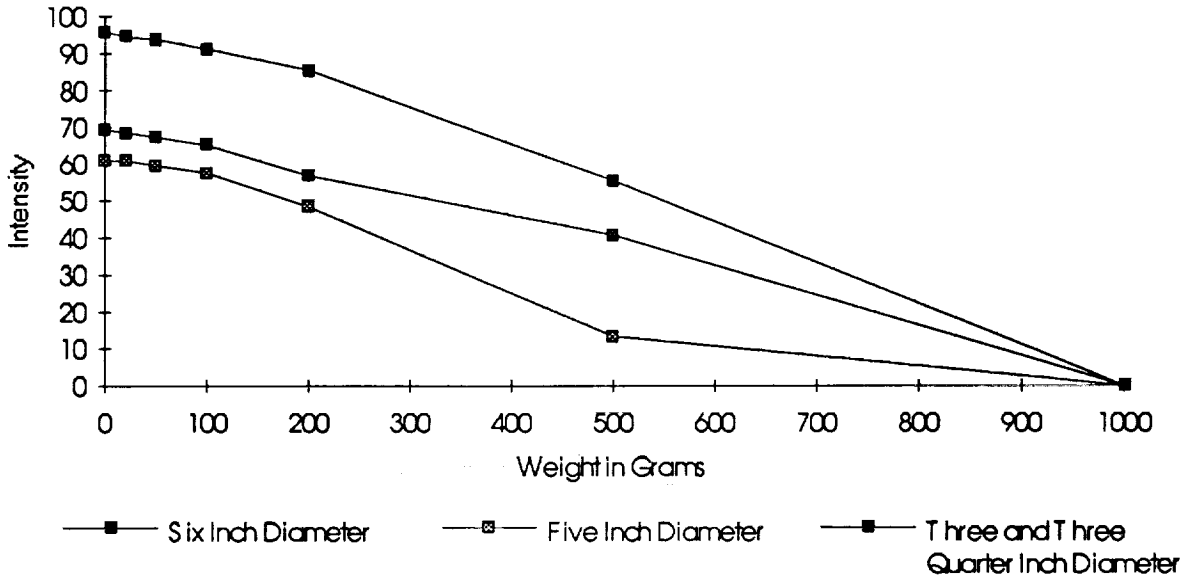

Figure 9. Analysis of the spatial frequency on the Corning 85/125/250 fiber.

As it can be seen from the plot, the three and three quarter inch circle was the most precise spatial frequency. It gives the largest dynamic range and the most linear output. Therefore, the spatial frequency for the vacuum system will have a greater number of spirals for the 10 inch diameter circle. This information was used as a baseline for the vacuum set up.

The set-up configuration for the vacuum system consisted of a B.T. & D. pigtailed laser diode and pigtailed detector, four Aurora Sure-Snap connectors and a fiber feedthrough. The connectors for the system is a very crucial part of the system. With the connectors that were used they were very sensitive to there position. If the connectors were moved to a different location or bumped the intensity could be decreased because there was not an efficient coupling of the fibers. It is crucial that the connections be the best possible. Another factor aiding the detection system would be the purchase of a amplifier for the photodiode.

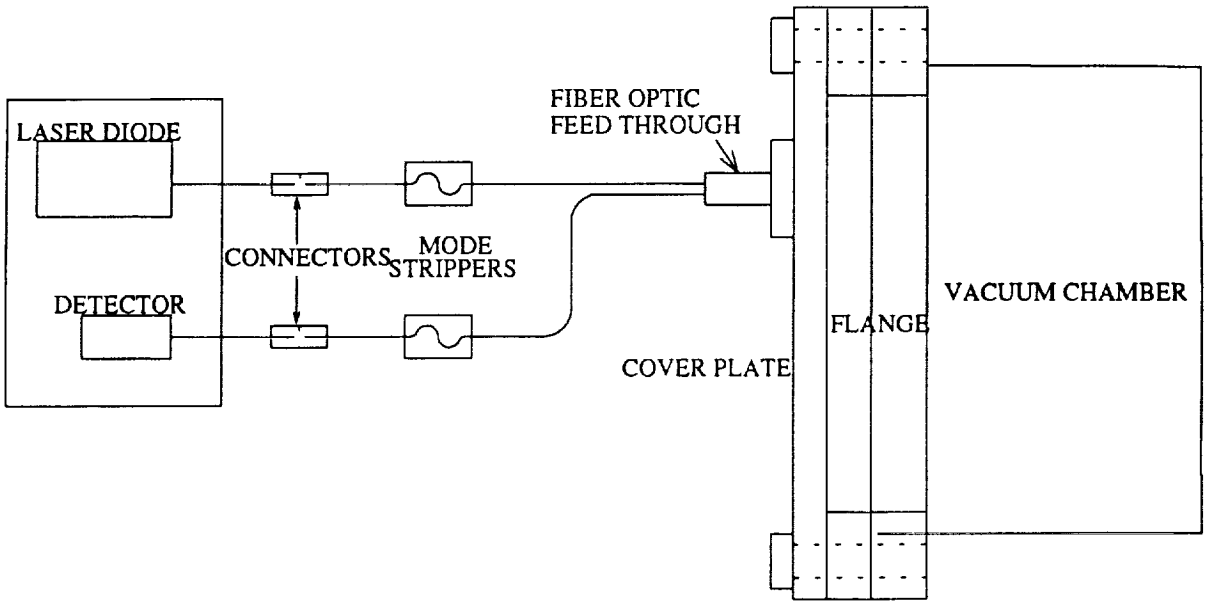

Figure 10. Microbend vacuum system.

The detector amplifier circuit can be found in Figure 11. The data was recorded using an A/D board monitoring the voltage of the Convectron vacuum gauge and the intensity of the infrared detector. Typically the data was obtained with an averaging rate of 850 readings per second.

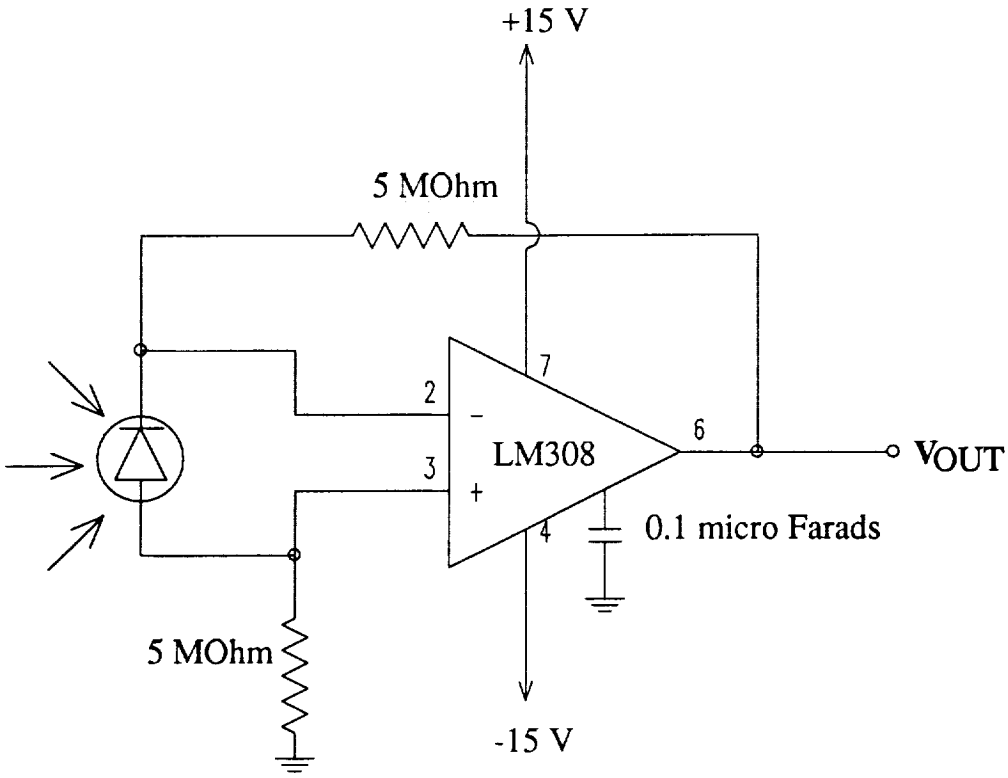

Figure 11. Photodiode detector amplifier circuit.

Once some characterization was made of the fibers, the fiber with the best response to the given weights was placed in the small vacuum chamber. The CeramOptech 100/110/130 fiber was not tested due to the fact that connectors for this small of a diameter fiber (130 micrometers) could not be found. Therefore, the Corning 85/125/250 CPC3 fiber was tested first. For this particular run there were 15 twists in the fiber. The vacuum was pumped down and the data was collected during the pump down with the computer. Although the output intensity of the sensor was not linear for the entire region, the system was responsive. The linearity, sensitivity and dynamic range can be improved by changing the spatial frequency of the spirals, adding mode stripping and mode scrambling, fiber characteristics and positioning of the fiber in the o-ring groove.

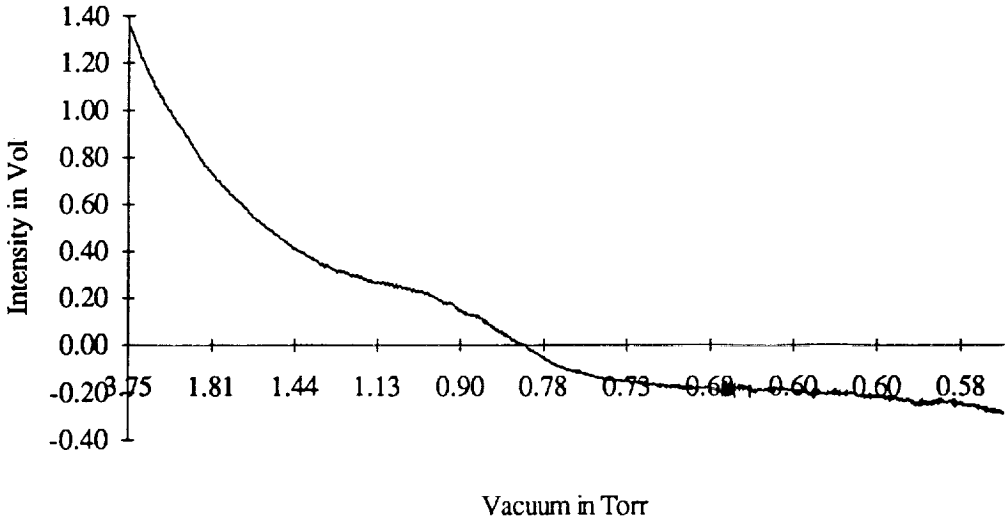

Figure 12. Corning 85/125/250 microbend sensor.

Figure 13 is a graphical representation for Figure 12 in decibel loss verses vacuum in Torr. With an initial intensity of 7.8 volts, at 750 milliTorr the loss is approximately 25 decibels and this loss decreases to 15 decibels at 3.75 Torr. In taking the log of the initial intensity over the output intensity the loss becomes a stair step function.

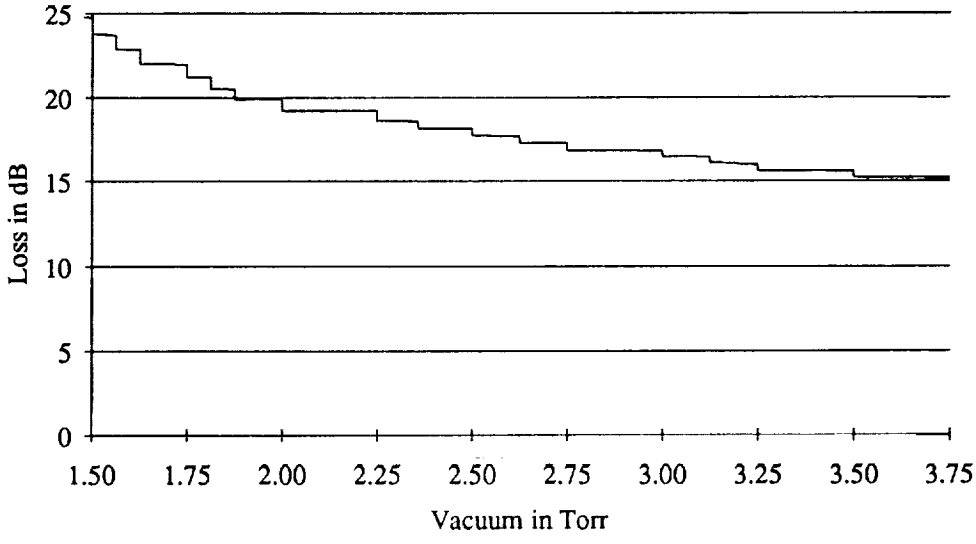

Figure 13. Loss verses Vacuum for Corning Fiber 100/140/250.

Another fiber that was tested was the Corning 100/140/250 CPC3 fiber. This fiber has a larger core and larger numerical aperture which was thought to aide in its microbending sensitivity. But because of this increase in sensitivity to microbending there was a much smaller dynamic range. For an instance, with the Corning 85/125/250 the range was from +10 volts to 0 volts when the lid was placed on the chamber and bolted down. In contrast when the vacuum system was closed and assembled with the Corning 100/140/250 fiber, the losses were so great that the output decreased from six volts without the cover to around three volts with the cover bolted in place. Therefore, there was a much smaller sensing range.

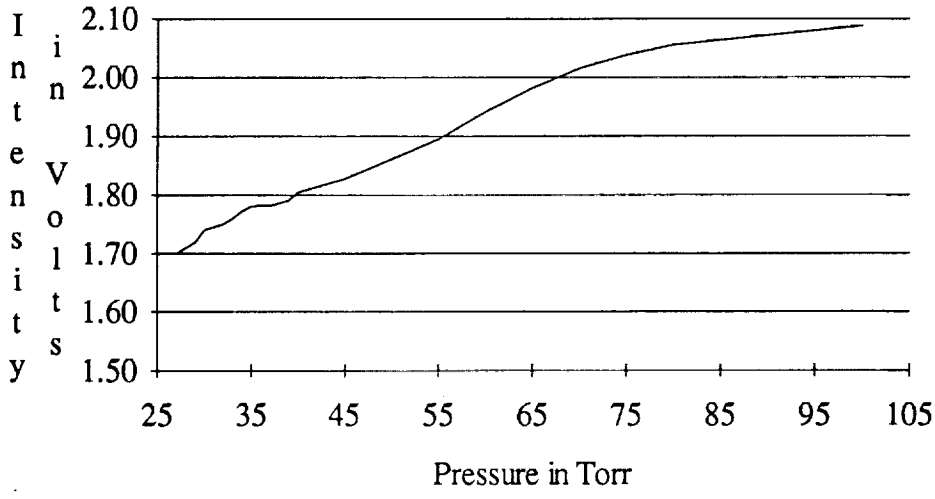

Figure 14. Corning 100/140/250 fiber microbend sensor.

The data taken above was taken during the leak up of the vacuum system. The sensor is responsive to the changes in the system. But it appears that there is too much loss before the system even begins to start pumping down. Improvement could be made by either or both method, buying a narrow band amplifier or by using a fiber with a different coating material. In this particular type of fiber the Corning 85/125/250 fiber appears to be more responsive for the range from 0.58 torr to 3.75 torr. While the Corning 100/140/250 fiber is responsive for a range from 25 Torr to 100 Torr with this particular set-up.

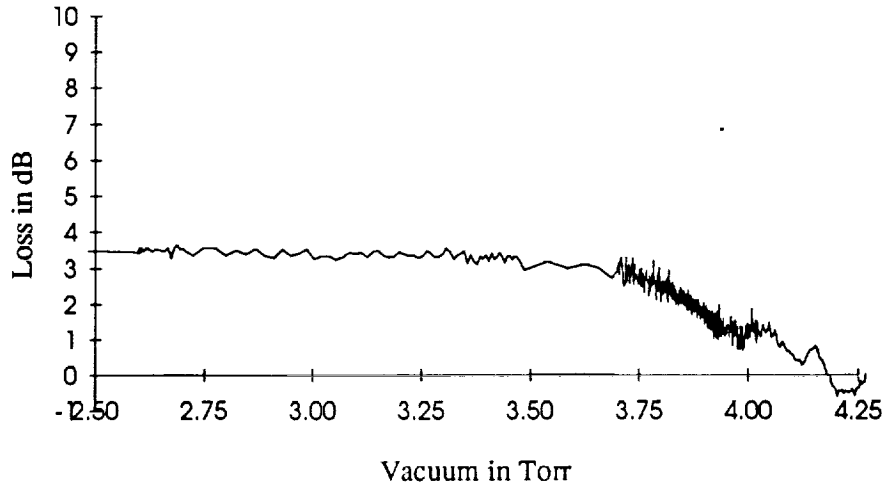

Figure 15. Loss verses Vacuum for Corning Fiber 100/140/250.

4.0 Conclusions

The use of optical fiber sensors for monitoring of seal integrity has been shown to be quite feasible. In this work two different optical fiber approaches were tested: microbending and Mach-Zehnder Interferometry. Both techniques showed merit in providing a response proportional to pressure changes due to known weights and to pressure changes in a vacuum o-ring seal gland. Each technique requires more work before it can be implemented into a useful concept. For example, in the microbending studies, we were not able to utilize an optical fiber which had been optimized for pressure monitoring applications. Samples of optical fiber which had been optimized for communications applications were available and used for these tests. Also note that polarization problems exist in the currently available Mach-Zehnder Interferometer that was used in this study. More work can be performed with polarization maintaining optical fiber to improve that experiment, as well as performing experiments with a two wavelength sensor as proposed by Dr. Abushagur in the appendix.

Other types of seals may be more useful for optical fiber sensors than the o-ring glands used in this work. For example the gask-o-seals proposed for space station would certainly be more easily embedded with an optical fiber sensor than an o-ring gland. Testing that has been performed revealed that the concept of embedding the optical fibers in the sealing material would help eliminate many problems including placement of the optical fiber, movement of the

optical fiber, modifications to the sealing faces, and other difficulties that can be attributed to retrofitting an optical fiber in an o-ring gland. Also note that using another material to over coat the twisted optical fiber would also eliminate certain difficulties in the task. This type of 'smart' or 'intelligent' seal would be very useful for almost any type of seal arrangement desired due to the compact size and the fact that there are no active elements. Optical fiber sensors are not limited to any particular pressure range. These sensors can be implemented into vacuum systems as well as high pressure systems. Flexibility occurs also in the diameter of the sealing fixture. The optical fiber sensors could be implemented in a small diameter Space Station vacuum seal as easily as it could be implemented in a SRM high pressure seal. Therefore not only is the fiber optic sensor a functional device, it is also very flexible. Continued research in fabrication of suitable fiber claddings and inter-connects will provide useful tools for monitoring and ensuring seal integrity.

5.0 Acknowledgements

The assistance of Mr. A. Bouzid and Z. He in performing the Mach-Zehnder interferometry experiments is greatly appreciated.

5.0 References

1. Murata, H., "Handbook of Optical Fibers and Cables", Dekker Press, New York, 1988
2. Daly, J. C. , "Fiber Optics", CRC Press, Boca Raton, 1984
3. Davis, C.M., et. al. "Fiber Optic Sensor Technology Handbook", pub. Optical Technologies, Inc., Herdon, VA 1986
4. Krohn, D. A., "Fiber Optic Sensors; Fundamentals and Applications, pub. by Instr. Soc. America, Research Park Triangle, 1988
5. Giallorenzi, T. G., et. al. "Optical Fiber Sensor Technology", IEEE, Q.E. 18 (1982) pp.626 - 665
6. G. Hocker, Opt. Soc. Am. 4, (1979) 320
7. Keck, D. B., "Fundamentals of Optical Waveguide Fibers", IEEE Comm., 23, (1985), pp 17-22.
8. Cielo, P. and J. Lapierre, "Fiber Optic Ultrasound Sensing for the Evaluation of Materials:, Appl. Optics 21 (1982) pp 572 - 575
9. Fields, J. N. and J. H. Cole, "Fiber microbend Acoustic Sensor", Appl. Optics 19 (1980) pp 3265 - 3267
10. Charasses, M. N., et. al. "Dynamic Pressure Sensing with a side-hole birefringment optical fiber", Op. Ltrs 16 (1991) pp 1043 - 1045
11. Olshansky, R. Applied Optics, 14 (1975) pp 20 -21
12. Personick, S.D., "Fiber Optics; Technology and Applications", Plenum Press, New York, 1985
13. Cheo, P.K., "Fiber Optics; Devices and Systems", Prentice-Hall, Englewood Cliffs, New Jersey, 1985
14. Musikant, S., "Optical Materials", Marcel Dekker, New York, 1985

6.0 Appendix

Introduction

Optical fibers enjoyed widespread of applications the last two decades, especially in communication systems. Some of their attractive properties are low losses, immunity from electromagnetic interference, and light weight. Over the recent years, fibers are being exploited for sensing in medical and industrial applications. Fibers can be used for both local and distributed sensing systems. They typically exhibit high sensitivity, good linearity, and a wide dynamic range[1,2]. A popular type of such sensors is the Fiber Optic Mach-Zehnder interferometer[1,2,3,4,5].

In this work, we focused on measuring "quasi-static" and dynamic pressure with both a F.O. Mach-Zehnder interferometer and a single-mode fiber. We investigated, first, the effect of such a pressure on a single-mode (SM) optical fiber. We found that, as predicted, anisotropic stress causes a birefringence in the fiber which in turn causes a change in the state of polarization (SOP) of the transmitted light. And, since this phenomenon has a directional asymmetry, it is sensitive to the input SOP of the light. Then, we used the F.O. Mach Zehnder interferometer to show that the isotropic and lateral components of the anisotropic static pressure are separable. Moreover, a piece of conventional single-mode fiber will suffice to detect the asymmetry in the sensed pressure.

We begin by outlining the theoretical design equations for isotropic and anisotropic linear sensing using phase and birefringence detectors such as fiber interferometers. Then, we present the results of our measurement of quasi-static and dynamic pressure, followed by a discussion and some suggestions of how to avoid polarization induced fading and low-frequency drift. We, also, present ideas of how to extend the dynamic range and sensitivity of the M-Z sensor to suit the needs of the present project. Two-wavelength sensing is particularly promising.

Theory

Pressure-induced Stress in a SM fiber:

An ideally round straight strain-free "single" mode fiber has two degenerate modes of propagation[6]. It, therefore, conserves the state of polarization(SOP) of light as it propagates through it. Thus, the angle of the SOP, θ, of a linearly polarized light (Fig. 1) remains unchanged as the latter is transmitted through such an ideal fiber. The effect of any anisotropic force exerted on such a fiber can be approximated by the superposition of the effects of the isotropic and the lateral components of such a force, Fig.2.

It can be shown, for this case, that the time varying output intensity is given by

$$E^2(t) = A^2\{\cos^2(\theta)\cos^2(\omega t+\phi) + \sin^2(\theta)\cos^2(\omega t+\phi+B)\} \quad (1)$$

where ϕ and B are phase differences induced by isotropic and lateral forces, f_i and f_{lat}, respectively. ϕ and B vary linearly with f_i and f_{lat}, respectively[3,6].

The lateral component, f_{lat}, of the force causes a birefringence[6] in the fiber and thus lifts the degeneracy in it. The birefringence, in turn, causes a change in the SOP of the light transmitted. An evaluation of such a change in the SOP is given by the apparent ellipticity defined as

$$e_a \equiv \left|\frac{I_{max}-I_{min}}{I_{max}+I_{min}}\right| = \sqrt{1-\sin^2(B)\sin^2(2\theta)} \quad (2)$$

where I_{max} and I_{min} are the time average of the maximum and the minimum of $E^2(t)$, respectively.

From equation (2), it is clear that for a non-zero angle of incidence of SOP, θ, small phase changes B induced by birefringence can be obtained from the measured apparent ellipticity; i.e. for a fixed non-zero θ,

$$B = \sin^{-1}\left[\sqrt{\frac{1-e_a^2}{\sin^2(2\theta)}}\right] \quad , \quad \text{Modulus } \pi. \quad (3)$$

Stress Measurement with a F.O. Mach Zehnder Interferometer

An interferometric fiber optical sensor converts acquired phase-modulated information into amplitude-modulated signal which can, then, be easily detected by photo-diode detectors. And in a two-arm mono-mode optical fiber sensor, the phase modulation is due to the physical sensitivity of the optical fiber to different fields such as pressure and temperature.

In the presence of pressure and temperature variations, ΔP and ΔT, the induced phase change between the sensing and reference arms of the interferometer is given by:

$$\Delta\phi = \frac{2\pi}{\lambda}(n\,\Delta L + L\,\Delta n) \quad (4)$$

where ΔL and Δn are the resultant changes in the length, L, and the index

of refraction, n, of the sensing fiber, respectively. λ is the wavelength of the light.

An anisotropic stress induces both a phase delay and a birefringence in the sensing arm of the F.O. Mach Zehnder interferometer(Fig. 4 .) The optical pathlengths of the two arms are nearly equal to within the coherence length of the source. Thus, the electric fields from the reference and the sensing arms interfere coherently to produce the following time-average intensity

$$I=\frac{I_0}{4}\left[\begin{array}{c}1+\cos^4(\theta)+\sin^4(\theta)+2\cos^2(\theta)\sin^2(\theta)\cos(B)\\ +2\cos^2(\theta)\cos(\phi)+2\sin^2(\theta)\cos(\phi+B)\end{array}\right] \quad (5)$$

where, as in equation (1), ϕ and B are phase differences introduced by isotropic and lateral stresses, respectively. A special case of equation (4), $\theta = 45^o$, is computed and plotted in Fig. 5; ϕ was, arbitrarily, chosen to be equal to 4B. The simplest case of equation (2) is (when $B=0$ .i.e. the pressure is isotropic):

$$I=\frac{I_0}{2}(1+\cos\phi) \quad (6)$$

Sensitivity and dynamic range:

For materials whose Poisson's ratio is close to 0.5 (ex: silicone, rubber, polyester,...), the dynamic range is limited by the following linearly measurable phase change[1,2]

$$\Delta\phi \approx \frac{2\pi}{\lambda} n(0.92)\, L\Delta P \quad (7)$$

Thus the sensitivity is linearly proportional to the length of the sensing fiber and the dynamic range is inversely proportional to it.

Experimental Results

1. Quasi-static pressure (Stress):

In these series of tests, we measured the response of a S.M. fiber and the M-Z to the stress induced by putting different weights on the sensing fiber. And, to convert weights to pressure values, we used the approximation that the pressure induced on a S.M. fiber by an isotropic force, W, is given by

$$P=\frac{W}{\pi d L} \quad (8)$$

where W is the weight in gram-force, d is the outside diameter of the fiber,

and L is the length of the portion of such a fiber under stress. For the S.M. fiber, we used, $d \equiv .250$ mm.

1.a Measurement using a S.M. fiber:

Fig.3 shows an experimental measurement of e_a. In such an experiment, we coupled a linearly polarized HeNe laser into a 15m-long single-mode optical fiber (Newport, SV). We, then, measured the output intensity as different weights were exerted vertically on a small section (9 mm-long) of the fiber.

As predicted by equation (2) for a fixed value of θ, the apparent ellipticity e_a in Fig.3 varies sinusoidally with the exerted pressure. However the minima approaching zero seem to be inconsistent with the simple prediction of equation (2). A possible explanation for such a discrepancy is that the state of polarization incident on the area under pressure is, in fact, elliptical due to the non-polarization-preserving fiber.

1.b Measurement using the M-Z interferometer:

Examples of measurement results of anisotropic stress using the F.O. Mach Zehnder interferometer are shown in Fig. 5.a and Fig. 5.b. Both plots are for a fixed input SOP. In Fig. 5.a, a small section (9mm) of the sensing arm was placed between two hard surfaces on which different weights are exerted. The interference intensity was, then, measured accordingly. In Fig. 5.a; however, a rubber band was wrapped around the section of the fiber under stress in an attempt to isotropically distribute the weight pressure.

As predicted theoretically (Fig.3), the measured intensity variation (Fig.5.a) shows two simultaneous sinusoidal responses to the exerted stress: A "carrier" and an "envelope". The former remains unchanged as the anisotropicity is removed when a rubber band is used. The latter, however, changes dramatically. The more the stress is axially isotropic, the longer the period of the envelope is. Thus, we conclude that the envelope of the plot in Fig. 5.a is primarily a result of the birefringence component of the phase change. Such an envelope has, obviously, expanded as the birefringence is decreased when a rubber band was used.

2. Dynamic Pressure:

2.a Using the M-Z:

In this experiment, we placed the sensing arm of the M-Z in the groove made to host the O-ring. As the inside of the chamber is evacuated using a vacuum pump, the O-ring squeezes the sensing fiber to the wall of the groove. The pressure exerted on the fiber is proportional to that

experienced by the O-ring. We, then, pumped the chamber down to 117 mTorr. We ran the experiment few times with the same set-up. An example of the measured response of the M-Z sensor is presented in Fig.6. The reason why the periods of the sinusoidal response is longer in the region (250 to 500 mTorr) is because, in that range the pumping was so fast that it is very difficult to monitor the response of the sensor.i.e. the data points read in such region may be too few.

Sensitivity and dynamic range: The measured sensitivity is 4.22L units/psi. and the measured dynamic range is .36/L psi.

2.b Using a SM fiber:

Here, we placed an approximately 1.3 m-long single mode fiber in the groove hosting the O-ring. At the output end, we placed a linear polarizer in front of the detector to measure the polarization changes. As theory predicts, the response is "sinusoidal" in addition to a d.c. value which depends on the input angle. In the experiment, we found that the response is very sensitive to the position of the fiber inside the groove (see Figs. .a and .c.) Such a change is caused by fiber bending which introduces extra phase delay in the fiber. If one avoids changing the initial position of the fiber, the result is fairly repeatable.

We, also, found that the input direction of the SOP changes the shape of the response curve (see for example Figs. .a and .b.) This can be a calibration parameter fo the designer to center the linear response in the desired dynamic range. Introducing a twist to the leads of the sensor by rotating the chamber did not alter the response significantly (Figs. .c and .d.)

Sensitivity and dynamic range: The measured sensitivity is 0.044L units/psi. and the measured dynamic range is 10.6/L psi.

Analysis and discussion

a. Dynamic range/ Sensitivity: As anticipated, the M-Z is very sensitive to pressure variations and to thermal fluctuations. It is so because, like all interferometric sensors, it is a phase sensitive device. The directly measured range was about 32 psi using a 9mm sensing portion of the fiber. This is inversely proportional to such a length. So, using a longer sensing arm would reduce the dynamic range considerably (about .33 psi for L=1m.)

This result agrees with that reported by Davis et al.. However, Hocker

predicted a much higher dynamic range (from 16 to 28 psi-m.) We think that this big difference is because Hocker didn't account for the compressibility factor of the jacket around the fiber as Davis did.

b. Extension of the Dynamic Range:

1. By comparing the isotropic and anisotropic measurements, we notice that both the single fiber and the M-Z are sensitive to any birefringence induced in the sensing fiber. Such sensitivity is lower than that of the phase change. This suggests the possibility of using a single mode fiber to sense anisotropic pressure by detecting the change in the SOP. This should have a much wider dynamic range with less sensitivity.
2. One can, also, double the dynamic range by reading the intensity at one detector and monitoring the slope of change .i.e. measuring the time derivative.
3. Similarly, since the light intensity alternates sinusoidally between detector 1 and detector 2 (Fig.1), as the phase difference is increased, taking the difference between both read intensities doubles the sensitivity of the sensor without decreasing the dynamic range. This way, the device will be twice as sensitive to noise.
4. The dynamic range can be increased by decreasing the phase sensitivity. This can be achieved, for example, by using longer wavelengths or a fiber with a different material whose index of refraction is less sensitive to pressure.
5. Polarization-maintaining (PM) fibers are less sensitive to pressure. So, a single PM fiber or an interferometer made of such fibers should have a wider range.

c. PIF and low frequency noise:

Polarization induced fading (PIF) is a problem common to all interferometric sensors. This fading, or visibility of the fringes approaching zero, happens as the input SOP is changed or if there is a difference in the SOP of both arms of an interferometer. The visibility is zero (no interference) when the SOP's of both arms are orthogonal to each other. Different techniques ranging from feedback controls to optical compensation were proposed and tested to avoid the problem.

On the other hand, low frequency drifting due to thermal fluctuations in the environment and or phase noise in the source has been observed in virtually all interferometric fiber sensors. Such noise is even worse if the difference in fiber length in both arms is bigger.

D. A. Jackson et al showed that the low frequency drift in a single mode all-fiber interferometer can be eliminated using a servo-driven piezo-

electrically stretched coiled fiber. However, this controller was designed for signal band (100Hz-10KHz.)

We observed regular drifts of about 1.2 10^{-3} Hz in the all-fiber interferometer which we used to generate pressure data. And, we observed a drift of the interference fringes with much longer period (freq. = 9.3 10^{-5} Hz) on another M-Z set-up consisting of a He-Ne laser beam split in two equal beams which, in turn, were each coupled to a SM fiber (1m-long). The other ends of such fibers are, then, placed side by side to form the interference fringes.

d.Simultaneous sensing of pressure and temperature (Fig.7):
Two-wavelength sensing allows us to measure pressure and temperature Simultaneously with an extension of the dynamic range and without losing the sensitivity offered by interferometric sensors.

Pressure and temperature are inter-related and so, their effects on a single mode fiber are similar. So, it is difficult to completely separate them using interferometric fiber optic sensors. Few techniques have been proposed. We suggest that by, simultaneously using two wavelengths in the same M-Z interferometer and thus obtaining two responses for the same temperature and pressure changes, we should be able to solve for these two unknowns. Besides allowing us to separate temperature and pressure, such a technique permits us to extend the dynamic range of the sensor considerably. This can be achieved by calculating the difference between the two responses. Referring to equation (4) and assuming that the changes in the index of refraction and in the length of the sensing fiber are the same at both wavelengths , then such responses are given by

$$\Delta\phi_1 = \frac{2\pi}{\lambda 1}(n\,\Delta L + L\,\Delta n) \tag{5}$$

$$\Delta\phi_2 = \frac{2\pi}{\lambda_2}(n\,\Delta L + L\,\Delta n) \tag{6}$$

where λ_1 and λ_2 are the two wavelengths. And so,

$$|\Delta\phi_1 - \Delta\phi_2| = \frac{2\pi}{\lambda\, equ}(n\,\Delta L + L\,\Delta n) \tag{7}$$

where,

$$\lambda_{equ} = \frac{\lambda_1 \lambda_2}{|\lambda_1 - \lambda_2|} \tag{8}$$

λ_{equ} is much longer than either λ_1 or λ_2 if they are close enough. As an example, for λ_1 = .6328 um and λ_2 = .830 um, $\lambda_{equ} = 4.21\lambda_1$.

References

1. C. M. Davis, " Fiber Optic sensors: an overview," Opt. Engineering, vol. 24, p. 347, 1985.
2. A. D. Kersey, " Recent progress in interferometric Fiber Sensor technology," SPIE vol. 1367 Fiber Optic and Laser sensors VIII (1990).
3. G. B. Hocker, " Fiber Optic sensing of pressure and temperature," Appl. Opt., vol. 19, p. 1445, 1979.
4. A.D. Kersey, A. Dandridge, and M. J. Marrone, " Optimization and stabilization of fringe visibility in interferometric sensors using input polarization control," J. Lightwave Technol., vol. 6, p. 1599, 1988.
5. A. D. Kersey, M. J. Marrone, and A. Dandridge, " Analysis of input polarization-induced phase noise in interferometric Fiber-Optic sensors and its reduction using polarization scrambling," J. Lightwave Tech., vol. 8, p. 838, 1990.
6. L. B. Jeunhomme, by Marcel Dekker Inc., (1990), chapter 2.
7. A. Simon and R. Ulrich, " Evolution of polarization along a single mode fiber," Appl. Phys. Lett., vol. 31, p. 517, 1977.
8. A. G. Barlow, " Quadrature Phase Shift Technique for measurement of strain, optical power transmission, and length in optical fibers," J. of Lightwave Tech., vol. 7, p. 1264, 1989.
9. R. Ulrich, S. C. Rashleigh, and W. Eickhoff, " Bending-induced birefringence in single mode fibers," Opt. Lett., vol. 5, p. 273, 1980.
10. M. N. Charasse, M. Turpin, and J. P. LePesant, " Dynamic Pressure sensing with a side-hole birefringent optical fiber," Opt. Lett., vol. 16, p. 1043, 1991.

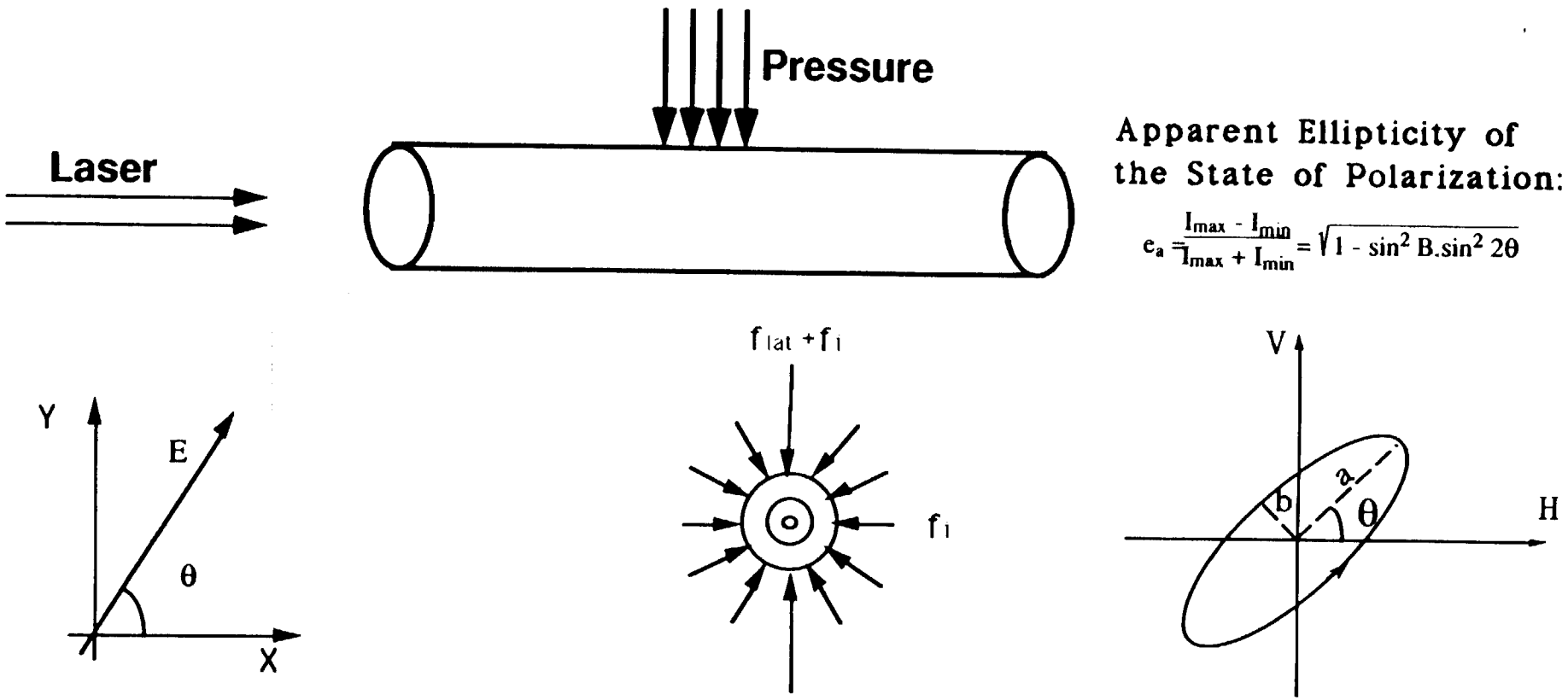

Fig.1: Effect of pressure on a single-mode fiber

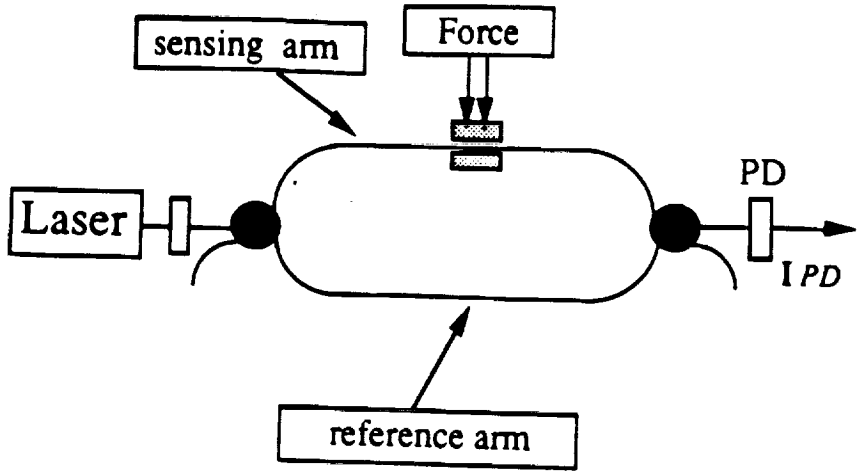

Fig. 2: Mach-Zehnder Interferometer

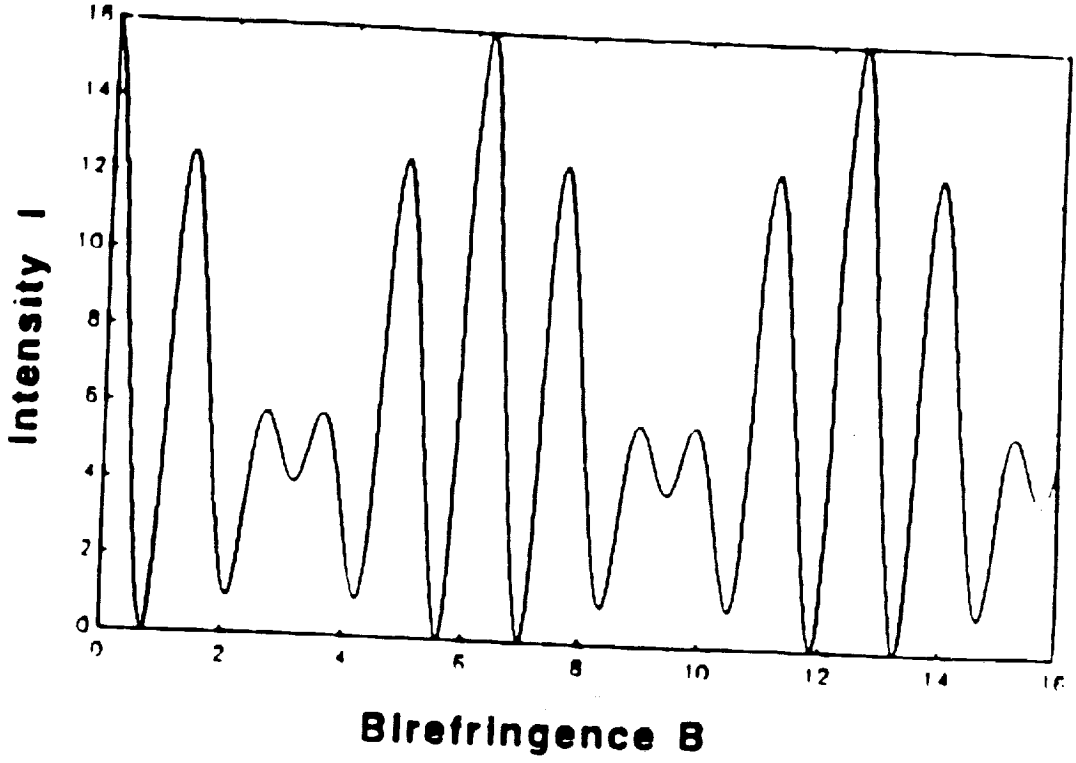

Fig. 3: Simulated Mach-Zehnder sensor output; $\theta = 45^{o}$ and $\phi = 4B$.

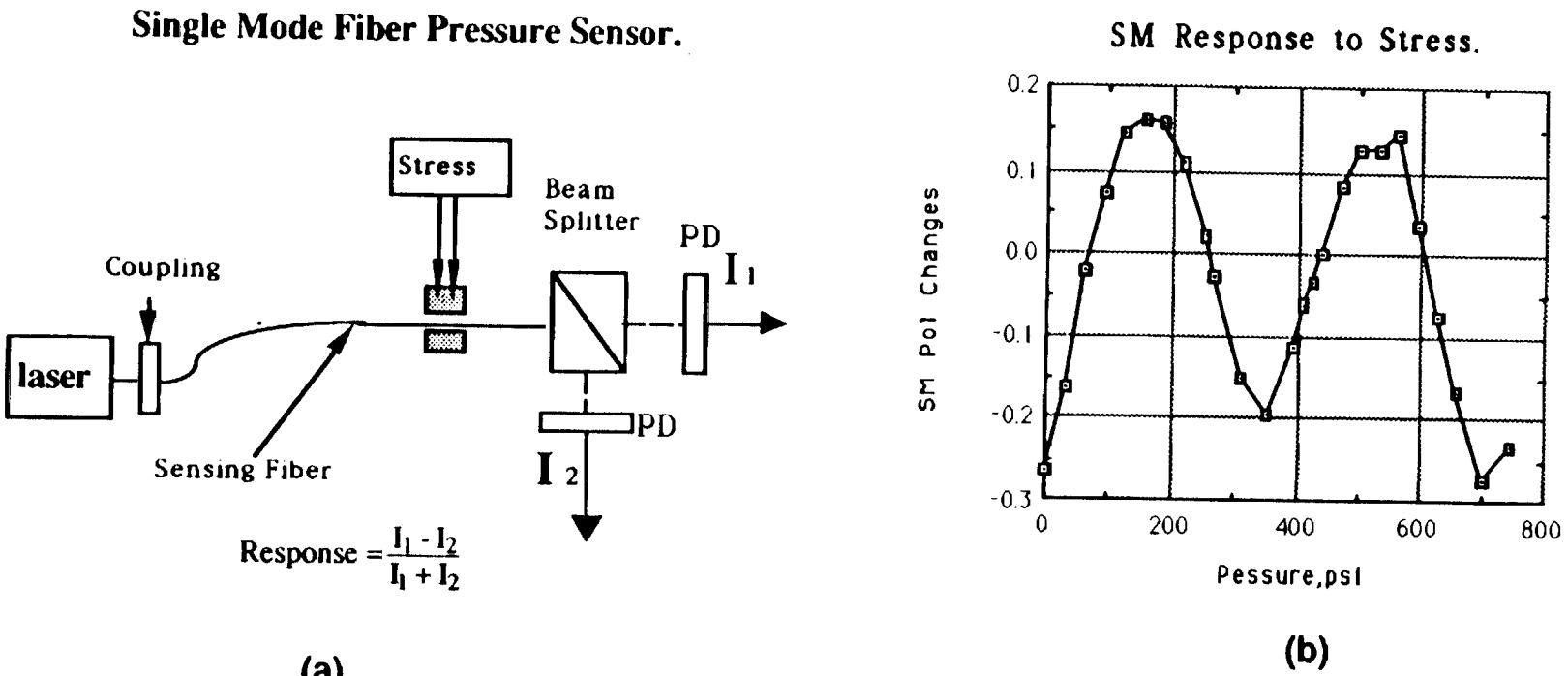

Fig.4: Measurement of "quasi-static" pressure using a single-mode fiber

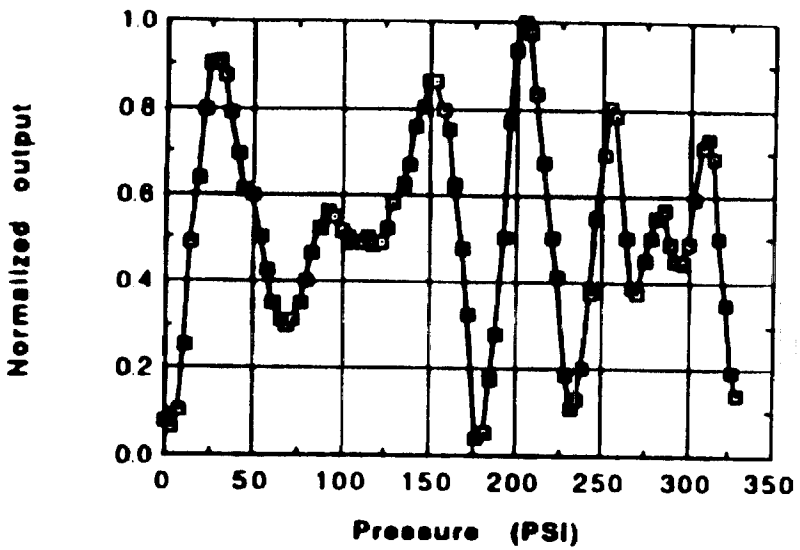

(a)

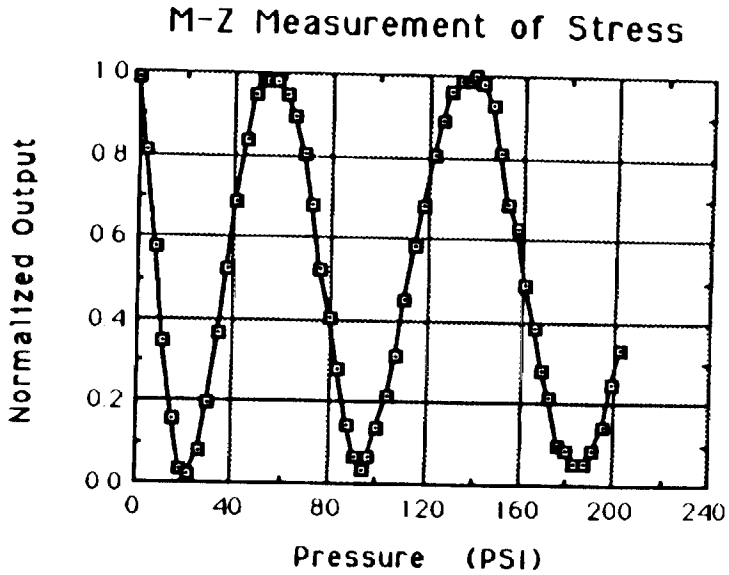

(b)

Fig. 5: Measurement of "quasi-static" pressure using the Mach-Zehnder interferometer.

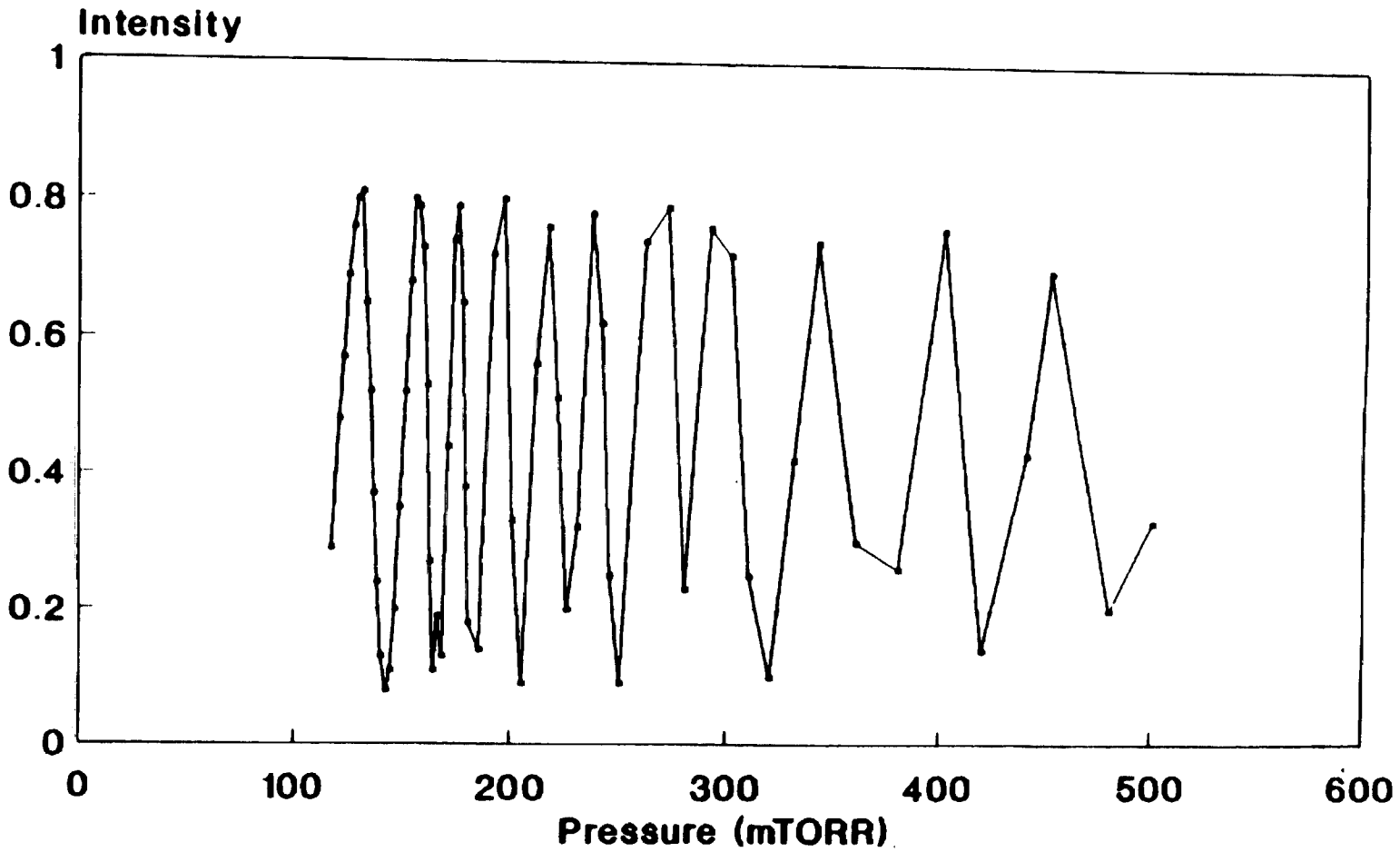

Fig.6: Measurement of dynamic pressure using a Mach-Zehnder interferometer in a high vacum chamber.
Length of sensing fiber is about 1 m.

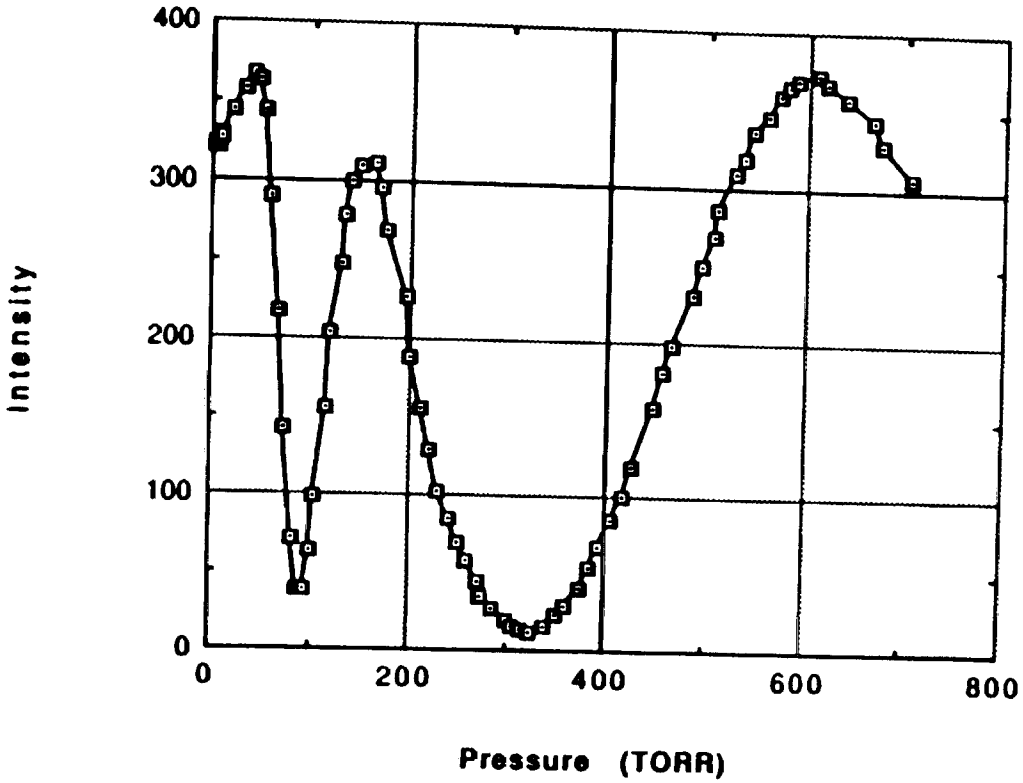
Intensity
400
300
200
100
0
0
200
400
600
800
Pressure (TORR)

Fig. 7a

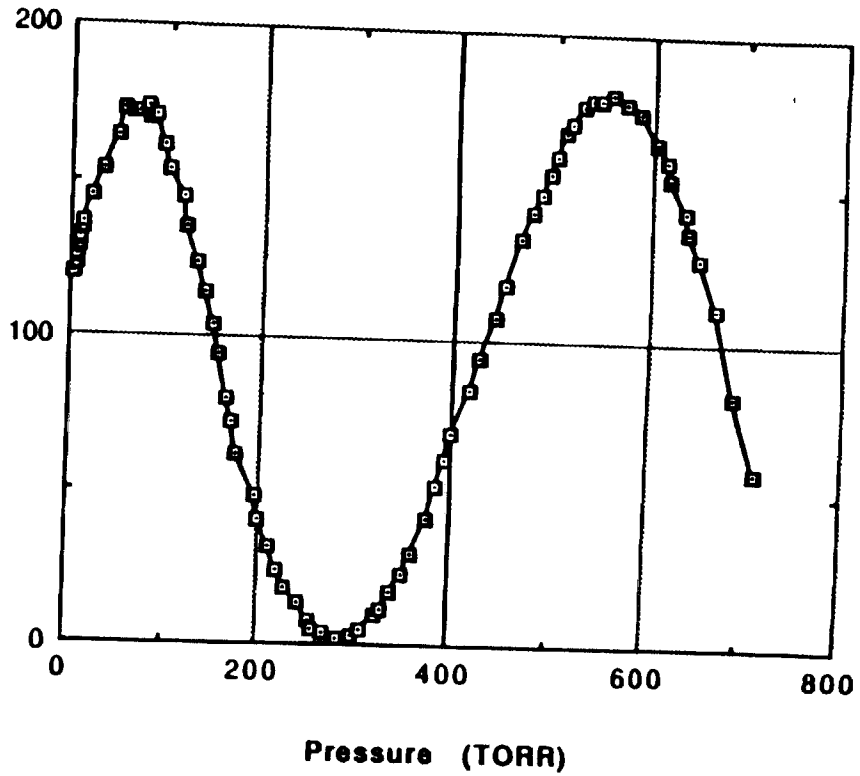
200
100
0
0
200
400
600
800
Pressure (TORR)

Fig. 7b

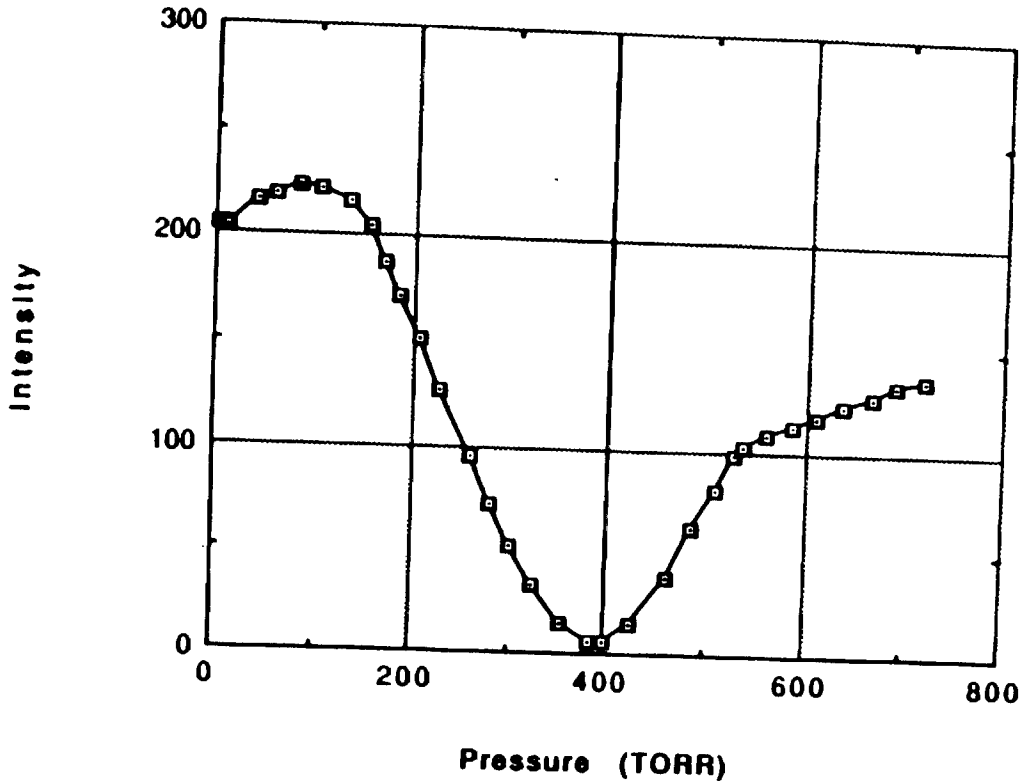
Intensity
300
200
100
0
0
200
400
600
800
Pressure (TORR)

Fig. 7c.

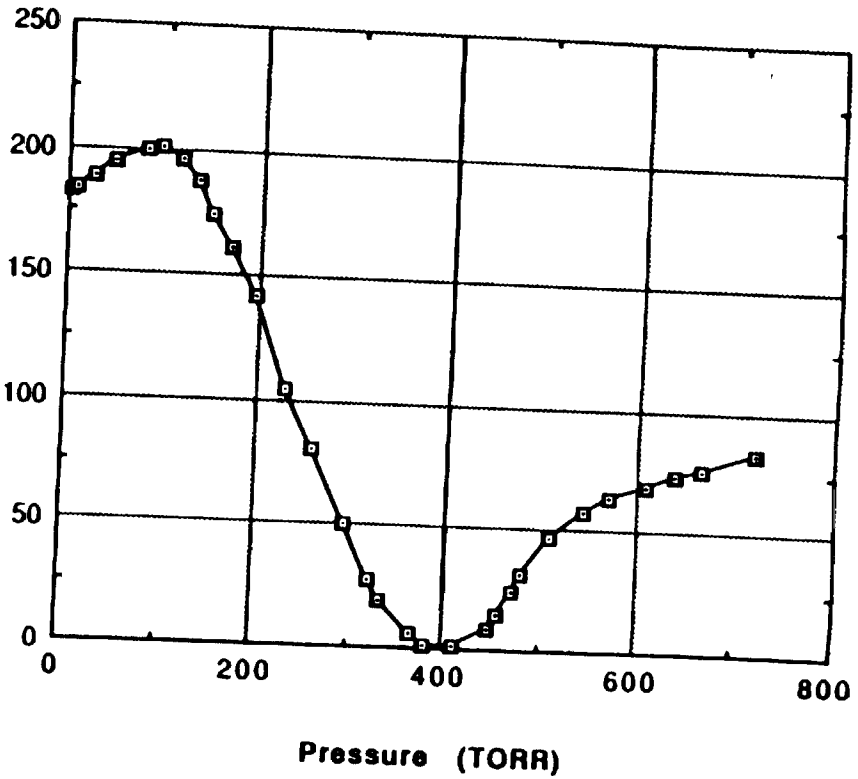
250
200
150
100
50
0
0
200
400
600
800
Pressure (TORR)

Fig. 7d

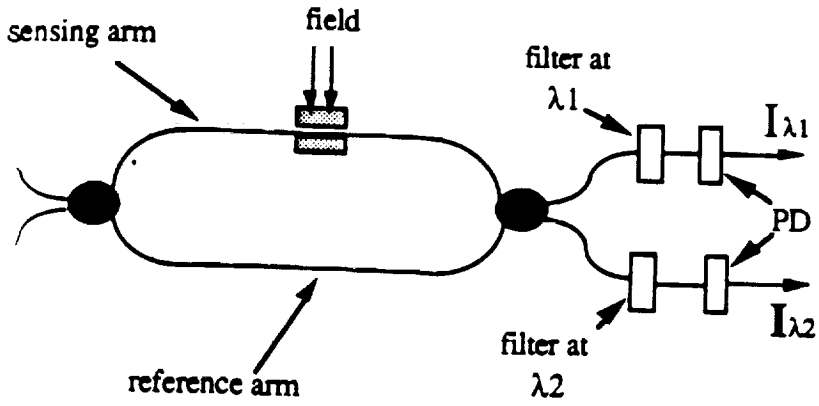

- Wavelength Mach - Zehnder Interferometer